Report No. 394

DEVELOPMENT OF THE SEMI-EMPIRICAL AMMONIA DEPOSITION AND EMISSION (SEADE) MODEL FOR APPLICATION TO NORTH CAROLINA WATERSHEDS

By
Dr. John T. Walker[2], Mr. Robert E. Austin[1] and Dr. Wayne P. Robarge[1]

[1]Department of Soil Science
College of Agriculture and Life Sciences
North Carolina State University
Raleigh, North Carolina

[2]U.S. Environmental Protection Agency
National Risk Management Research Laboratory
Air Pollution Prevention and Control Division
Research Triangle Park, NC

May 2010

UNC-WRRI-394

DEVELOPMENT OF THE SEMI-EMPIRICAL AMMONIA DEPOSITION AND EMISSION (SEADE) MODEL FOR APPLICATION TO NORTH CAROLINA WATERSHEDS

Dr. John T. Walker, Mr. Robert E. Austin and Dr. Wayne P. Robarge

Department of Soil Science
College of Agriculture and Life Sciences
North Carolina State University
Raleigh, NC 27695

The research on which this report is based was supported by funds provided by the North Carolina General Assembly through the North Carolina Department of Environment and Natural Resources.

This report fulfills the requirements for a project completion report of the Water Resources Research Institute of The University of North Carolina. The authors are solely responsible for the content and completeness of the report.

WRRI Project No. 70240
May 2010

ACKNOWLEDGMENTS

Many individuals and organizations contributed to the success of this project. Elin Arnaudin and Kim Whitley provided the expertise needed to visually validate and develop the emissions inventory from the Confined Animal Feedlot Operations (CAFO) database. The North Carolina Division of Water Quality Aquifer Protection Section provided the base animal operations data used to develop the emission inventory and Keith Larick provided answers to many of our CAFO's related questions. Data quality control and preliminary data processing were administered by Sue Kimbrough of the Environmental Protection Agency. We appreciate the field support of Wayne Fowler and Alf Wall (EPA). Finally, we thank the Water Resources Research Institute for funding this research and for their help and support.

Funding for this project was provided by the North Carolina Water Resources Research Institute.

ABSTRACT

Globally, domestic animals are the largest source (22 Tg N yr-1, 1 Tg = 10^{12} g) of atmospheric NH_3, comprising approximately 40% of natural and anthropogenic emissions combined, while synthetic fertilizers and agricultural crops together contribute an additional 12.6 Tg NH_3-N y^{-1} (23% of total emissions) (Bouwman et al., 1997). Within and downwind of agricultural regions, NHx therefore represents a significant fraction of atmospherically derived N entering terrestrial and aquatic systems (Whitall and Paerl, 2001). While significant progress has been made in determining wet deposition inputs of NHx to eastern North Carolina ecosystems, the magnitude of NH_3 dry deposition remains unknown. In this study, a new model for estimating NH_3 dry deposition at field to watershed scales in areas of intensive animal production is presented. The Semi-Empirical Ammonia Deposition and Emission (SEADE) Model is used to produce an initial watershed scale estimate of NH_3 dry deposition which takes into account the bi-directional nature of NH_3 air-surface exchange with vegetation, soils, and water and resolves spatial features, such as concentration and deposition gradients around individual animal facilities that are missed by larger regional air quality models. The SEADE model consists of three components: 1) a facility-scale NH_3 emission inventory; 2) a spatial model for predicting atmospheric NH_3 concentrations; and 3) a model for predicting net NH_3 air-surface transfer rates. The model domain for this study includes the Neuse and Cape Fear river basins located within the coastal plain of North Carolina. The facility-scale NH_3 emissions inventory was created using the North Carolina Department of Environment and Natural Resources, Division of Water Quality (NCDWQ) Confined Animal Feedlot Operations database and a visual verification procedure via aerial imagery. Three different ground level NH_3 concentration models following the form of a shifted power law ($y = ax^k + \varepsilon$) were tested and analyzed. Model I was developed from weekly integrated concentrations measured along horizontal gradients from 10 to 700m downwind of a 5000 animal swine facility (Walker et al., 2008). Models II and III were validated using data from the Carolina Ammonia Monitoring Network (CAMNet) using a split-sample approach. Results from the calibration and validation procedure indicate that Model I most closely predicts the observed NH_3 concentrations (RMSE = 3.3 µg m^{-3}). The air-surface exchange of NH_3 (flux) is calculated using the two-layer canopy compensation point model developed by Nemitz et al. (2001), in which the competing processes of emission and deposition within the foliage-soil (or water) system are taken into account by relating the net canopy-scale NH_3 flux (F_t) to the net emission potential of the canopy (i.e., foliage and soil or water), or surface concentration (χ_o). The air-surface exchange model predicts a total net dry deposition of 20.6 million kg NH_3, 6.9 million kg within the Neuse and 13.6 million kg within the Cape Fear, an estimated 37% of the total atmospheric nitrogen deposited within the Neuse and Cape Fear basin. Uncertainty analysis indicates a high degree of model sensitivity to the stomatal compensation (χ_s) and soil/water compensation (χ_g) points.

TABLE OF CONTENTS

ACKNOWLEDGMENTS iii
ABSTRACT iv
TABLE OF CONTENTS v
LIST OF FIGURES vii
LIST OF TABLES ix
SUMMARY AND CONCLUSIONS x
RECOMMENDATIONS xii
1. INTRODUCTION 1
1.1 Background 1
1.2 Study Objectives 2
2. METHODS 2
2.1 Model Description 2
2.1.1 Emission Inventory 2
2.1.2 Atmospheric Ammonia Concentrations 4
2.1.2.1 Models 4
2.1.2.2 Observations 5
2.1.3 Ammonia Air-Surface Exchange Model 9
2.2 Model Implementation 12
3. RESULTS 13
3.1 Model Calibration 13
3.1.1 Atmospheric Concentrations 13
3.1.2 Ammonia Air-Surface Exchange Model 16
3.2 Model Validation 17
3.2.1 Emissions Inventory 17
3.2.2 Ammonia Concentration Model 20
3.3 Watershed-scale Concentration Distributions 27
3.4 Watershed-scale Deposition 31
3.5 Nitrogen Deposition Budget for the Neuse and Cape Fear River Basins 40
3.6 Model Uncertainty and Sensitivity 41

4. FUTURE WORK 43
5. REFERENCES 44
APPENDIX 46

LIST OF FIGURES

Figure 1: Location of CAMNET monitoring stations used to calibrate the monthly emission factor for ground level ammonia concentration. 6

Figure 2: The yearly average NH_3 concentration measured during the Lizzie and CAMNet studies (Walker, *et al.*, 2000b). Concentrations decrease exponentially with distance from the nearest animal facility. 13

Figure 3: Yearly average NH_3 concentration in air for each of the 23 CAMNet monitoring stations. The average seasonal minimum and maximums are show as error bars. 14

Figure 4: Linear model illustrating the concentration of ammonia in air versus the distance to the nearest animal facility for each of the modeled seasons. 15

Figure 5: Average 24-hour profile for daytime air temperate and soil moisture for each of the 4 seasons modeled. Air temperature is shown as a solid line, soil moisture as a dotted line. 16

Figure 6: Average seasonal 24-hour profile wind speed used in the air-surface exchange model. 17

Figure 7: Number of Broilers produced per county as reported by the North Carolina Department of Agriculture and Consumer Services (NCDA&CS, 2006). 19

Figure 8: Predicted concentration versus observed for Model I. Best fit line shown in black with 95% confidence intervals. 21

Figure 9: Predicted concentration versus observed for Model II. Best fit line shown in black with 95% confidence intervals. 22

Figure 10: Predicted concentration versus observed for Model III. Best fit line shown in black with 95% confidence intervals. 23

Figure 11: Comparison of seasonal mean observed concentrations (1 standard deviation) at remote CAMNet site P15 to seasonal minimum predicted concentrations in the Neuse and Cape Fear River basins 24

Figure 12: Relationship between the distance to the nearest NH_3 emission source and the magnitude of the prediction error. 26

Figure 13: Average seasonal concentrations for the Neuse River Basin as predicted by Model I. 29

Figure 14: Average seasonal concentrations for the Cape Fear River Basin as predicted by Model I. 30

Figure 15: Deposition versus distance from nearest animal facility as predicted by SEADE..... 31

Figure 16: Total seasonal ammonia flux for the Neuse river basin as predicted by the air-surface exchange model. Positive values indicate emission. 33

Figure 17: Total seasonal ammonia flux for the Cape Fear river basin as predicted by the air-surface exchange model. Positive values indicate emission. 34

Figure 18: Average and total air-surface exchange of ammonia by county. Counties with less that 20% of their area within the study area are excluded from the maps. 36

Figure 19: Land use classifications used in the air-surface exchange model for the Neuse and Cape Fear river basins. 37

Figure 20: Seasonal fluxes by land use category at high and low atmospheric NH_3 concentrations. Negative values represent deposition. 39

Figure 21: Concentration versus distance to the nearest animal facility for the 24 CAMNet stations used to calibrate and validate the SEADE model. Figures are provided for each of the four seasons. 48

LIST OF TABLES

Table 1: Variables tested and their significance in the parameterization of the concentration model. ($\alpha = 0.05$). Significant values are highlighted in bold. 14

Table 2: Various forms of the distance-decay, shifted power law function used to predict the average seasonal surface concentration of ammonia (NH_3) in air ($\mu g/m^3$)..... 16

Table 3: Comparison between the number of swine reported by the NCDA&CS and that of the CAFO's-based emissions inventory. The top 8 swine producing counties are shown. 18

Table 4: Comparison between the total yearly NH_3 emissions as calculated within SEADE and as calculated from the county-level production numbers reported by the North Carolina Department of Agriculture Statistics (NCDAS) Service. 20

Table 5: Seasonal model performance metrics: mean bias (MB, $\mu g\ m^{-3}$), normalized mean bias (NMB, %), root mean square error (RMSE, $\mu g\ m^{-3}$), normalized mean error (NME, %), and correlation coefficient (r). 21

Table 6: Total net dry deposition of NH_3 by season for the Neuse and Cape Fear river basins as predicted by the ammonia air-surface exchange model. 35

Table 7: Summary of seasonal dry NH_3 flux predicted by the air-surface exchange model by land cover classification. Negative values represent deposition to the surface, positive values represent emission from the canopy to the atmosphere. 38

Table 8: Atmospheric nitrogen deposition budget for the Cape Fear and Neuse River Basins.... 41

Table 9:Uncertainty in the predicted air-surface exchange of ammonia. 42

Table 10: CAMNet stations used to calibrate and validate the concentration component of the SEASE Model. 46

Table 11: Emission factors used to develop inventory for eastern North Carolina (Asman, 1992) 46

Table 12: Land use specific inputs by season used in the air-surface exchange. 47

SUMMARY AND CONCLUSIONS

Globally, domestic animals are the largest source (22 Tg N yr-1, 1 Tg = 10^{12} g) of atmospheric NH_3, comprising approximately 40% of natural and anthropogenic emissions combined, while synthetic fertilizers and agricultural crops together contribute an additional 12.6 Tg NH_3-N y-1 (23% of total emissions) (Bouwman et al., 1997). Within and downwind of agricultural regions, NHx therefore represents a significant fraction of atmospherically derived N entering terrestrial and aquatic systems (Whitall and Paerl, 2001). While significant progress has been made in determining wet deposition inputs of NHx to eastern North Carolina ecosystems, the magnitude of NH_3 dry deposition remains unknown. Measurements of ambient NH_3 concentrations across eastern North Carolina suggest the potential for high dry deposition rates in areas densely populated by animal production facilities (Robarge et al., 2002; Walker et al., 2004).

This study presents a new model for estimating NH_3 dry deposition at field to watershed scales in areas of intensive animal production, taking the Neuse and Cape Fear River basins as an initial case study. The SEADE model consists of three components: 1) a facility-scale NH_3 emission inventory; 2) a spatial model for predicting atmospheric HN_3 concentrations; and 3) a model for predicting net NH_3 air-surface transfer rates. This approach produces an initial watershed scale estimate of NH_3 dry deposition which accounts for the bi-directional nature of NH_3 air-surface exchange with vegetation, soils, and water and resolves spatial features, such as concentration and deposition gradients around individual animal facilities that are missed by larger regional air quality models.

The facility-scale NH_3 emission inventory was developed from the North Carolina Department of Environment and Natural Resources, Division of Water Quality (NCDWQ) Registration Database. To validate facility locations, the animal operations were overlaid with the Farm Services Agency (FSA) 2006 National Areal Imagery Program (NAIP) imagery and manually rectified within a Geographic Information System (GIS). Comparison between the CAFO-based emissions inventory and the independently collected statistics from the North Carolina Department of Agriculture Statistics (NCDAS) service provides an estimate of total basin-wide NH_3 swine emission within 6 percent of the SEADE emissions inventory.

Atmospheric NH_3 concentrations are calculated as a function of distance from the nearest animal production facility. Three different distance-decay models, following the form of a shifted power law ($y = ax^k + \varepsilon$), were compared for their ability to predict ground level NH_3 air concentrations. Model I was developed from weekly integrated concentrations measured along horizontal gradients from 10 to 700m downwind of a 5000 animal swine facility (Walker et al., 2008), Model II varied *a* by month using the same procedure as Model I but varied the decay exponent *k* by season. Model III used a fixed seasonal coefficient *a* and applied the same seasonally derived decay exponent *k* as used in Model II. Model performance was evaluated using the regression coefficient, mean bias (MB), normalized mean bias (NMB), root mean

square error (RMSE), and normalized mean error (NME). For Model I, regression plots revealed strong correlation between model and observations and followed a pattern of model overestimation at low concentrations and underestimation at high concentrations. In particular, mean bias ranged from -1.49 μg NH_3 m^{-3} in the winter to 2.1 μg NH_3 m^{-3} in the summer, indicating that the model tended to overestimate during warm months and underestimate during cold months.

In this study, NH_3 air-surface exchange (flux) is calculated using the two-layer canopy compensation point model developed by Nemitz et al. (2001), in which the competing processes of emission and deposition within the foliage-soil (or water) system are taken into account by relating the net canopy-scale NH_3 flux (F_t) to the net emission potential of the canopy (i.e., foliage and soil or water), or surface concentration (χ_o). The air-surface exchange fluxes are calculated by land use according to the 2001 National Land Cover Data imagery classification, which contains 21 land use classes at 30m horizontal resolution (NLCD, 2001). The model is driven with hourly meteorological data from the nearest NC State Climate Office AGNet station (NCSCO, 2007).

For the year, the air-surface exchange model predicted a net dry deposition totaling 20.6 million kg NH_3, 6.9 million kg within the Neuse and 13.6 million kg within the Cape Fear. In the Neuse, deposition averaged 1.2, 0.9, 1.2, and 0.6 kg ha^{-1} for the spring, summer, fall, and winter respectively. In the Cape Fear, deposition averaged 1.3, 1.3, 1.4, and 0.6 kg ha^{-1} respectively. On an annual scale, NH_3 is deposited to low nitrogen systems (forests, wetlands) and emitted from high nitrogen (fertilized) systems (cultivated crops, pasture).

Total deposition to both river basins was 20.6 million kg NH_3 on an annual scale, which represents 36% of total emissions calculated from the SEADE emissions inventory and 27% of total emissions calculated from the NCDAS database. Thus, the majority of NH_3 emitted within the two river basins is either wet deposited or transported out of the river basins.

Based on this study, it is concluded that a semi-empirical model that spatially predicts NH_3 emission and deposition is capable of capturing dry NH_3 at field-to-watershed scales in areas of intensive animal production and on a seasonal basis. With a further refinement of the emissions inventory, increased sampling regime, and additional improvements in the compensation point for different land cover classes, this model offers great promise in linking the complex, field-scale mechanistic processes with the large, regional-scale deposition models.

RECOMMENDATIONS

1. Further refinement of the emissions inventory would provide more accurate model predictions. New versions of the emissions inventory should include poultry and cattle facilities and should further split swine facilities when multiple lagoons are present. These refinements would enhance the prediction of the NH_3 concentration field and reduce uncertainty in areas heavily populated with poultry facilities.

2. The model presented here is limited in its ability to predict ground level air concentrations due to a relatively small number of measurement sites available for development and evaluation. Additional ALPHA passive samplers placed along transects from both poultry and swine operations would provide the information needed to refine the concentration model based on animal type. The current model was calibrated using observations from a solitary swine facility. Inclusion of measurements from poultry operations would enhance the ability to predict NH_3 concentrations over a greater range of animal types. Sampling both small and very large animal facilities would help expand the concentration model boundary conditions. Additional samplers placed outside the influence of animal operations would help refine baseline seasonal background NH_3 concentrations. Additional concentration measurements were taken at 25 different sites in 2008 – 2009. The next version of the model will employ these additional data for development and testing of the air concentration model.

3. Forthcoming analyses will also further compare and refine the 3 air concentration models examined here using additional field observations. As described below, the model produces a distribution of air concentrations at each model grid point consisting of N observations equal to the number of animal facilities within the model domain. In this analysis only the maximum concentration is retained, assuming that the nearest animal facility dominates the seasonal average concentration. Forthcoming analyses will examine other approaches, such as a summed concentration weighted by distance to the corresponding facility. Forthcoming analyses may also examine the performance of traditional dispersion models (Gaussian, Lagrangian).

4. Additional studies surrounding the compensation point for different land cover classes are urgently needed. As shown in this analysis, net fluxes are strongly influenced by the soil and vegetation emission potential (gamma). A database of soil/leaf gamma values, developed from direct measurements of leaf apoplast and soil solution hydrogen and ammonium ion concentrations, for primary land use categories is needed.

5. Improved parameterizations of the leaf cuticular resistance that are representative of primary vegetation types are also needed. Currently used parameterizations were developed from European experiments and their applicability to U.S. conditions and vegetation types has not be proven. New parameterizations may be developed from controlled fumigation experiments or field flux measurements.

6. Additional direct measurements of NH_3 air-surface exchange, using appropriate micrometeorological techniques, are needed to evaluate models such as the one presented here. Such measurements are expensive and heavily labor intensive and, as evidenced in this analysis, must include extensive process-level ancillary measurements for thorough interpretation and model development. Forthcoming analyses will compare modeled fluxes to limited available measured fluxes over eastern North Carolina (grass, forest, crops).

1. INTRODUCTION

1.1 BACKGROUND

Globally, domestic animals are the largest source (22 Tg N yr-1, 1 Tg = 10^{12} g) of atmospheric NH_3, comprising approximately 40% of natural and anthropogenic emissions combined, while synthetic fertilizers and agricultural crops together contribute an additional 12.6 Tg NH_3-N y^{-1} (23% of total emissions) (Bouwman et al., 1997). Within and downwind of agricultural regions, NHx therefore represents a significant fraction of atmospherically derived N entering terrestrial and aquatic systems (Whitall and Paerl, 2001). In natural systems where N is the limiting nutrient, atmospherically derived reactive N may have beneficial effects on productivity, including increased photosynthesis (Sievering et al., 2000) and accumulation of inorganic soil N (Padgett et al., 1999). Recent studies also indicate that enhanced N deposition may increase the carbon storage capacity of temperate forests (Sievering, 1999). When N input exceeds system requirements, however, environmental stresses such as soil acidification (Roelofs et al., 1985), forest decline (Nihlgard, 1985), and eutrophication of surface waters (Paerl, 1995; Paerl and Whitall, 1999) may occur. During the 1990's, the Coastal Plain region of North Carolina experienced a significant increase in agricultural NH_3 emissions, owing primarily to growth in swine and poultry populations (Walker et al., 2000a), which are most concentrated in the Cape Fear and Neuse River basins. Beginning with the increase in NH_3 emissions, the concentration of NH_4^+ in precipitation also increased significantly in this part of the state (Walker et al., 2000a; Walker et al., 2000b; Paerl and Whitall, 1999). Whitall and Paerl (2001) estimate that atmospheric wet deposition contributes 20 to 40% of biologically available “new” nitrogen entering North Carolina coastal waters. Furthermore, Paerl and Whitall (1999) report that high atmospheric nitrogen deposition rates are generally coincident with regions experiencing harmful algal bloom expansion, a symptom of eutrophication.

While significant progress has been made in determining wet deposition inputs of NHx to eastern North Carolina ecosystems, the magnitude of NH_3 dry deposition remains unknown. Measurements of ambient NH3 concentrations across eastern North Carolina suggest the potential for high dry deposition rates in areas densely populated by animal production facilities (Robarge et al., 2002; Walker et al., 2004). In a recent study at a swine facility in eastern North Carolina, Walker et al. (2008) estimated that approximately 10% of NH_3 emissions from the barns/lagoon complex were deposited within 500m downwind. Dry deposition rates > 50 kg N ha^{-1} yr^{-1} were predicted for distances < 100 m from the emissions complex, which included a forested riparian area. At 500 m from the source, dry NH_3 deposition was 16 kg N ha^{-1} yr^{-1}, which was approximately 3.5X wet deposition of NH_4^+. These results suggests that dry NH_3 deposition exceeds the critical nitrogen load (Kuylenstierna et al., 1998) for ecosystems in the vicinity of animal production facilities. The contribution of NH_3 dry deposition to total N deposition in North Carolina coastal watersheds, however, remains unknown. Without information on the magnitude and spatial variability of NH_3 deposition in mixed agricultural

regions (i.e., crop and animal production), assessments of ecosystem health and the potential for nitrogen saturation/eutrophication are incomplete.

1.2 STUDY OBJECTIVES

This study presents a new model for estimating NH_3 dry deposition at field to watershed scales in areas of intensive animal production, taking the Neuse and Cape Fear River basins as an initial case study. This approach will produce an initial watershed scale estimate of NH_3 dry deposition which takes into account the bi-directional nature of NH_3 air-surface exchange with vegetation, soils, and water and resolves spatial features, such as concentration and deposition gradients around individual animal facilities that are currently missed by larger regional air quality models.

The specific objectives of this study are to:

1. provide annual watershed scale estimates of NH_3 dry deposition for the Cape Fear and Neuse River basins;
2. estimate seasonal NH_3 concentration and net air-surface exchange fluxes at 100 m horizontal resolution within the model domain;
3. summarize the net NH_3 fluxes by primary land use type, counties, and across seasons;
4. establish an atmospheric nitrogen deposition budget for the Cape Fear and Neuse River basins;
5. evaluate the SEADE model with respect to ambient concentration predictions;
6. provide recommendations for continued model development and future research.

2. METHODS

2.1 MODEL DESCRIPTION

The SEADE model consists of three components: 1) a facility-scale NH_3 emission inventory; 2) a spatial model for predicting atmospheric NH_3 concentrations; and 3) a model for predicting net NH_3 air-surface transfer rates. The model is described in detail in the following sections.

2.1.1 Emission Inventory

Ammonia emissions are calculated for individual animal production facilities included in the North Carolina Department of Environment and Natural Resources, Division of Water Quality (NCDWQ) Registration Database. Operations include those deemed permitted under 15ANCAC2H.0217 Rule for Waste Not Discharged to Surface Waters. Animal operations are registered under this rule if the facility serves 250 or more swine, 100 or more confined cattle, 75 or more horses, 1000 or more sheep, or 30,000 or more confined poultry and are using a liquid waste management system. An annual emission rate is calculated for each facility based on the number and type of animals as described below. Annual emissions are scaled by an average monthly temperature to partition the emissions into a monthly inventory. The results of Walker et al., 2004 show that the NH_3 emissions budget for the Neuse and Cape Fear River basins is

dominated by swine (60% of total) followed in importance by turkeys (10%), chickens (9%), cows (8%), and fertilizer (6.5%).

To account for differences in per-swine emissions resulting from feed formulations used in phase feeding programs, emissions are calculated for each of the 19 facility types contained in the DWQ database using a combination of emission factors for boar stud/gilts (11.0 kg NH_3 animal^{-1} yr^{-1}; Asman, 1992), sows (16.43 kg NH_3 animal^{-1} yr^{-1}; van der Hoek, 1998), and fattening (market) hogs (6.39 kg NH_3 animal^{-1} yr^{-1}; van der Hoek, 1998). Where a combination of sows and fattening pigs are present, the following calculation is used:

$$ER_T = \left(DC_T \times CF \times FOS \times BEF_S\right) + \left(DC_T \times CF \times FMH \times BEF_{MH}\right) \quad (1)$$

where ER_T is the facility scale annual emission rate (kg NH_3 yr^{-1}); DC_T is facility design capacity in number of animals, CF is a correction factor for actual percent capacity, assumed to be 0.95, FOS is the fraction of sows present (0.1), and FMH is the fraction of market hogs present (0.9); BEF_S is the basic emission factor for sows (kg NH_3 animal^{-1} yr^{-1}) and BEF_{MH} is the basic emission factor for market hogs (kg NH_3 animal^{-1} yr^{-1}). The fraction of sows and market hogs is calculated from the most recent North Carolina market statistics (NCDACS, 2007).

When only one animal type is present at a facility, the annual emission rate reduces to

$$ER_T = DC_T \times CF \times BEF_T \quad (2)$$

where BEF_T is the basic emission factor for animal type T. Basic emission factors for the remaining animal categories, including cattle (e.g., milk, beef), horses, sheep, goats, and poultry (e.g., pullets, layers, broilers, and turkeys) are taken from Asman, 1992.

Although very few poultry facilities are contained in the CAFO's database, a yearly emission estimate for poultry was needed for model calibration. In 10 out of 24 sites the closest facility to a CAMNet site was a poultry house as determined from aerial imagery. From the imagery we are able to determine the number of barns contained by the facility, however, due to the lack of permit data we were unable to determine the type of house (e.g. layer, pullet, turkey, or broiler). As such, an average yearly emission of 0.4 kg NH_3 bird^{-1} yr^{-1}was used to best estimate the emissions from these facilities.

To account for seasonal variability, annual emissions are monthly allocated by scaling with ambient temperature (Walker et al., 2008). A linear regression model of the form

$$E_i = a_o - \alpha \cos\left(\frac{2\pi i}{12}\right) - \beta \sin\left(\frac{2\pi i}{12}\right) \quad (3)$$

is used to estimate the facility scale NH_3 emission rate (kg) for month *i* (E_i), where a_o is the average monthly emission rate in kg NH_3 (annual emission/12). Coefficients α and β are given by

$$\alpha = -8.9\left(\frac{a_o}{T}\right) \text{ and } \beta = -5.6\left(\frac{a_o}{T}\right) \quad (4)$$

where T is the average annual temperature (ºC)

2.1.2 Atmospheric Ammonia Concentrations

2.1.2.1 Models. Atmospheric NH_3 concentrations are calculated as a function of distance from the nearest animal production facility. Three different distance-decay models, following the form of a shifted power law ($y = ax^k + \varepsilon$), were compared for their ability to predict ground level NH_3 air concentrations. The main advantage of the shifted power-law formulation is its accuracy over a broader range of distance than that of logarithmic law formulation (Zou et al., 2006). The models were compared to analyze the effects of both the exponential decay constant *k* and the initial emissions coefficient *a*.

Model I was developed from weekly integrated concentrations measured along horizontal gradients from 10 to 700m downwind of a 5000 animal swine facility (Walker et al., 2008) and takes the form

$$NH_3 = a_j X^{-0.75} \quad (5)$$

Coefficient *a* in equation (5) varies by month as a result of the seasonality in emissions. The results of Walker et al. (2008) were used to derive the following relationship between the coefficient *a* and monthly emissions ($R^2 = 0.82$)

$$a_j = 0.29E_i + 35.1 \quad (6)$$

where E_i is monthly emission in units of kg NH_3 at facility *j*. The intercept was not statistically significant at p = 0.01 and is therefore set to zero.

Model II varies *a* by month using the same procedure as Model I but varies the decay exponent *k* by season. Model III uses a fixed seasonal coefficient *a* and applies the same seasonally derived decay exponent *k* as used in Model II. As described below, Models II and III were developed from the CAMNet database (see section 2.1.2.2).

Model validation measures were derived both externally (Model I) and internally (Models II and III). An external model validation was performed on Model I, developed from an independent

dataset (Walker et al., 2008) to CAMNet observations. Models II and III were developed and validated (internally) using only the CAMNet data in a split-sample approach. In general, an external model validation provides a more robust evaluation of model performance, however, it is considered reasonable to use internal model validation to calculate internal measures of validation such as the prediction error (Hastie et al, 2001). For Models II and III, the monitoring sites were divided into two sets of data, two-thirds of the sites (16 stations) for calibration and one-third of the sites (8 stations) for model validation. Because the concentration model is highly dependent on the distance to the nearest animal facility it was important to subset the data so that the calibration data contained sites with a full range of distances to the closest animal facility. To ensure that the model remained robust in regards to the distance to the nearest animal facility yet unbiased in the selection of calibration sites, the CAMNet sites were ordered by their distance to the nearest facility and then broken into 8 sets of 3 stations. A random number generator was used to pick one station out of each set of 3 that would be used for validation, the other two used for model calibration (Appendix Table X).

Model performance was evaluated using the regression coefficient, mean bias (MB), normalized mean bias (NMB), root mean square error (RMSE), and normalized mean error (NME) according to the following equations:

$$\mathrm{MB} = \frac{1}{N}\sum_{1}^{N}(C_\mathrm{m} - C_\mathrm{o}),$$

$$\mathrm{NMB} = \frac{\sum_{1}^{N}(C_\mathrm{m} - C_\mathrm{o})}{\sum_{1}^{N} C_\mathrm{o}} 100\%,$$

$$\mathrm{RMSE} = \sqrt{\frac{1}{N}\sum_{1}^{N}(C_\mathrm{m} - C_\mathrm{o})^2},$$

$$\mathrm{NME} = \frac{\sum_{1}^{N}|C_\mathrm{m} - C_\mathrm{o}|}{\sum_{1}^{N} C_\mathrm{o}} 100\%, \qquad (7a – 7d)$$

where Cm and Co represent model and observed concentrations, respectively.

2.1.2.2 Observations

The Carolina Ammonia Monitoring Network (CAMNet), which is operated by investigators Walker and Robarge, consists of 24 monitoring sites within the Cape Fear and Neuse River basins at which weekly integrated NH_3 concentrations are measured at ground level using passive air samplers (Figure 1). Samplers were positioned to measure NH_3 concentrations in the vicinity of different types of animal facilities and at a range of distances from 100 to 4500 meters away. The sites were positioned in random directions from the nearest facility and in various

landscape settings. Of the 24 sites, 10 sites were located closest to poultry operations, 14 closest to swine. The size of the facilities ranged from a 12 barn poultry facility to a 27,000 feeder-to-finish swine operation.

Figure 1: Location of CAMNET monitoring stations used to calibrate the monthly emission factor for ground level ammonia concentration.

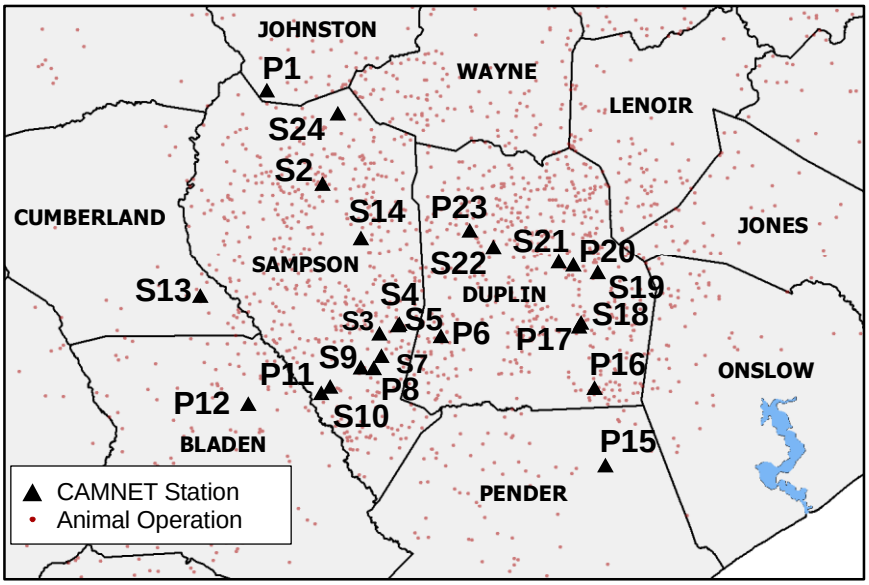

Ground level NH_3 air concentrations were measured with the ALPHA passive sampler (Tang et al., 2001). The sampler consists of a 6 mm long, 21 mm inner diameter FEP Teflon tube. One end contains a 5µm PTFE membrane, through which NH_3 gas diffuses and is adsorbed onto an acid-coated collection filter located at the other end of the diffusion path. The membrane prohibits particle collection and thus the NH_3 concentration is not biased high by collection of ammonium aerosol. The membrane also forms a quasi-laminar layer of air adjacent to its outer surface which serves to establish a turbulence-free diffusion path between the membrane and the collection filter, thus avoiding "wind-shortening" of the diffusion path. Within CAMNet, samplers were deployed in replicate (2) for 1 to 2 weeks at each measurement location (Figure 1) in an open bottom rain shelter fixed at a height of 1.5 m above ground.

The ambient concentration of NH_3 determined by the passive sampler depends on the mass of NH_3 adsorbed by the collection filter, exposure duration, and diffusion coefficient. The mass of NH_3 adsorbed by the collection filter is calculated by:

$$Q = (c_e - c_b)v \qquad (8)$$

where v is the volume of the extract (mL), c_e is the filter extract concentration of NH_4^+ (μg mL^{-1}), and c_b is the extract concentration of an unexposed travel blank (μg mL^{-1}). Each batch (weekly or biweekly) of samples is bracketed by two sets of $N = 6$ travel blanks, which account for contamination during transport to and from the field site. In this case, c_b represents the median of these two sets of travel blanks.

The concentration of NH_3 in air is then calculated as:

$$[NH_3] = Q/V \quad (9)$$

where V is the effective volume of air sampled (L). The theoretical volume of air sampled is:

$$V = DAt/L \quad (10)$$

where D is the temperature dependent diffusion coefficient of NH_3 in air (Massman, 1998), A is the tube cross sectional area (mm^2), t is the time of exposure, and L is the length of the diffusion tube (mm).

Collection filters (25 mm, Swiftlab, UK) were coated with a solution of 5% (w/w) phosphorous acid in methanol. Exposed collection filters were extracted in 2.5 mL deionized water and stored at 4 ^oC prior to analysis by ion chromatograph (Dionex model DX-120, Dionex, Sunnyvale, CA). Laboratory and field (travel blanks) were analyzed along with field-exposed samples. Six laboratory blanks were processed for each batch (defined by weekly or biweekly sampler deployment period) of field exposed samples and represent extracts from samplers that are prepared in the laboratory using standard procedures then extracted immediately and stored at 4 ^oC until analysis. Six field blanks were processed for each batch of field exposed samples and represent extracts from unexposed samplers that are transported to and from the field sites with field exposed samplers. The travel blank characterizes all sources of contamination and variability related to laboratory procedures and transport to and from the field site.

Previous studies with passive devices have shown that the effective sampling rate (S)

$$S = DA/L = V/t \quad (11)$$

is lower than the theoretical value due to additional resistance to diffusion by the PTFE membrane at the sampler entrance (Tang et al., 2001). The sampling rate must therefore be characterized and calibrated over the range of sampling conditions (i.e., NH_3 concentration, duration of exposure, etc.) either by field comparison to an independent reference method (Tang et al., 2009) or exposure to a known concentration of NH_3 under controlled conditions. By quantifying the mass (Q) of NH_3 collected by the sampler at a particular air concentration [NH_3]

and exposure period (t), equations (9) and (11) can be solved for the effective sampling volume (V) and uptake rate (S), respectively. Finally, by monitoring temperature during exposure, an adjustment to the diffusion coefficient (D) may be derived using equation (10).

Similar to the approach of Walker et al. (2008), we characterized the uptake rate (S) by exposing the ALPHA sampler to a range of NH_3 concentrations (1 to 100 $\mu g\ m^{-3}$) in a well-mixed Teflon-lined 61cm(L)×30.5cm(W)×19cm(H) acrylic chamber over exposure periods ranging from 1 – 7 days. Ammonia concentrations were generated by mixing NH_3 (10 ppm ± 5% or 100 ppm ± 5%; Airgas; Durham, NC) with clean air via calibrated mass flow controllers or critical orifice. The concentration of NH_3 in air entering and exiting the chamber was monitored using a dual-cell Pranalytica photoacoustic NH_3 detector (Nitrolux Model 200; Pranalytica, Inc.; Santa Monica, CA). Our experiments yield a median value (N = 40) of $S = 0.00356 \pm 0.00015\ m^{-3}\ hr^{-1}$, which agrees closely with the value of $0.00324\ m^{-3}\ hr^{-1}$ obtained by Tang et al. (2009) via field comparison to the to the DELTA denuder system (Sutton et al., 2001). The primary sources of uncertainty in our calculation are accuracy of the reported NH_3 cylinder concentration (±5%) and the precision of the passive sampler during the exposure experiments (8%), yielding a total uncertainty ≈ 9.5%, which is on the same order as the difference (9.4%) between our estimate of S and that of Tang et al. (2009).

Detection limit, or minimum detectable concentration (L_D), was calculated as a function of the standard deviation of field blanks (σ_o) as outlined by Currie (1999)

$$L_D = 2t_{1-\alpha,\upsilon}\sigma_o \qquad (12)$$

where t is the Student's t-statistic with υ degrees of freedom and a 5% probability of accepting the alternative hypothesis "analyte present" when it is false (α= 0.05). Equation (12) assumes constant variance between L = 0 and $L = L_D$ and a 5% probability of accepting the null hypothesis "analyte absent" when it is false (β = 0.05). Because the batchwise variance of the travel blank is not constant over time, L_D is determined for each batch of N = 6 travel blanks. Method precision was determined as the median absolute relative difference between collocated duplicate samples.

Accuracy of the ALPHA sampler was assessed by comparison to phosphorous acid coated glass (URG Corp., Chapel Hill, NC) annular denuders (U.S. EPA, 1997; Perrino and Gherardi, 1999). Denuders were operated for 24 hours at a mass flow controlled (URG Corp., Chapel Hill, NC) air sampling rate of 10 Lpm. Denuders were extracted with 10 mL deonized water and analyzed for NH_4^+ by ion chromatography (Dionex DX-120; Dionex, Sunnyvale, CA). ALPHA/denuder comparisons took place at Duke Forest, near Chapel Hill, NC, and the Clinton Horticultural Crops Research Station, near Clinton, NC (Site 14 [S14], Fig. 1), from January to November, 2009. The Duke Forest site is a suburban site characterized by relatively low NH_3 concentrations

(Sparks, et al., 2008) while the Clinton site is in an area of widespread animal and crop production and therefore experiences much higher NH_3 concentrations (Robarge et al., 2002). For this comparison, the mean and median daily denuder NH_3 concentrations during a weekly period containing N = 7 observations (i.e., denuders were not operated in replicate) was compared to the mean and median of N = 4 replicate ALPHA weekly measurements. Denuder precision during previous studies was < 10% expressed as coefficient of variation of replicates (Robarge et al., 2002; Bash et al., 2010).

Agreement between the two methods was assessed by calculating the median absolute relative percent difference between average concentrations and by reduced major axis regression. Ayers (2001) demonstrated in an analysis of air quality data that RMA was superior to ordinary least squares regression, which tends to underestimate the slope parameter and overestimate the intercept when both X and Y variables contain error. Regression analysis comparing weekly mean and median ALPHA and denuder samples (N = 72 observations) showed good agreement between the two methods. Slopes (± standard error) were 0.90±0.027 and 0.99±0.034 for mean and median weekly concentrations, respectively, and corresponding R^2 values were 0.94 and 0.92. Intercepts of 0.02 and 0.01 for mean and median concentrations, respectively, were not statistically significant (P > 0.1). The median absolute relative difference between average ALPHA and denuder concentrations was 0.29%, with highest values observed at concentrations below 0.25 μg NH_3 m^{-3}. At such low concentrations, the ALPHA concentration becomes increasingly sensitive to the blank correction, a problem that would be reduced to some degree for longer exposures (i.e., increasing ratio of exposed vs. blank concentration in sample extract).

The median LOD (48.0 μg NH_4^+-N L^{-1}, N = 48) is equivalent to 0.24 and 0.12 (μg NH_3 m^{-3}) in air for 1 and 2 week exposures, respectively, at 25°C. Sampler precision, defined as the median absolute relative percent difference (RPD) between duplicate samples, was 6.9% (N = 1081). RPD tends to increase with decreasing concentration below ≈ 1 μg NH_3 m^{-3}, reaching a median value of 30% for the 20 observations surrounding (10 above/10 below) the weekly detection limit of 0.24 μg NH_3 m^{-3}.

2.1.3 Ammonia Air-Surface Exchange Model

Ammonia may be either emitted from or deposited to vegetation, soil, and water, depending on the "compensation point" of the underlying surface. For this reason, the traditional approach of calculating deposition fluxes by applying a deposition velocity to the atmospheric concentration, which is appropriate for gases with a zero surface concentration such as sulfur dioxide and nitric acid (Fowler and Unsworth, 1979; Hicks et al., 1987), is not appropriate for NH_3 (Deerhake et al., 2005). For NH_3, a model framework that recognizes the bidirectional nature of the exchange process is required. In this study, NH_3 air-surface exchange (flux) is calculated using the two-layer canopy compensation point model developed by Nemitz et al. (2001), in which the competing processes of emission and deposition within the foliage-soil (or water) system are

taken into account by relating the net canopy-scale NH_3 flux (F_t) to the net emission potential of the canopy (i.e., foliage and soil or water), or surface concentration (χ_o). The system of equations describing the net canopy flux (F_t), as well as component fluxes [i.e., stomatal (F_s), cuticular (F_w), and ground (F_g)], is given by Nemitz et al. (2001).

Total and component fluxes are dependent on the canopy compensation point (χ_c), defined by Nemitz et al. (2001) as

$$\begin{aligned}\chi_c = [\chi_a (R_a R_b)^{-1} + \chi_s \{(R_a R_s)^{-1} + (R_b R_s)^{-1} + (R_g R_s)^{-1}\} + \chi_g (R_b R_g)^{-1}] \\ \times \{(R_a R_b)^{-1} + (R_a R_s)^{-1} + (R_a R_w)^{-1} + (R_b R_g)^{-1} + (R_b R_s)^{-1} \\ + (R_b R_w)^{-1} + (R_g R_s)^{-1} + (R_g R_w)^{-1}\}^{-1}\end{aligned} \quad (13)$$

where χ_a is the atmospheric NH_3 concentration, R_a is the atmospheric aerodynamic resistance, R_b is the atmospheric boundary layer resistance, R_s is the leaf stomatal resistance, R_w is the leaf cuticular resistance, and χ_s is the stomatal compensation point. NH_3 exchange with the ground is described by the soil compensation point (χ_g) and the ground resistance ($R_g = R_{ac} + R_{bg}$), which is determined by the in-canopy aerodynamic (R_{ac}) and ground boundary-layer resistances (R_{bg}). In the case of exchange over open water, the ground resistance reduce to zero.

Upon determination of χ_c, the surface concentration [$\chi(z_0)$] may be calculated according to

$$\chi(z_0) = \frac{\chi_a R_a^{-1} + \chi_g R_g^{-1} + \chi_c R_b^{-1}}{R_a^{-1} + R_b^{-1} + R_g^{-1}} \quad (14)$$

The net flux may then be calculated as

$$F_t = -\frac{\chi_a - \chi(z_0)}{R_a} \quad (15)$$

The aerodynamic resistance is calculated as a function of the standard deviation of wind direction (σ_θ), and wind speed (u) according to Hicks et al. (1987) assuming that the atmosphere is considered unstable when global radiation (G) exceeds 100 W m^{-2} (Meyers et al., 1998). The boundary-layer resistance is calculated according to Duyzer et al. (1992). Following Hicks et al.

(1987), friction velocity (u_*) is calculated from the near-neutral approximation as a function of R_a and u.

The bulk stomatal resistance to NH_3 transfer (R_s) is assumed equal to that of water vapor (H_2O) corrected for differences in molecular diffusivity. Stomatal resistance to H_2O is calculated as a function of G, air temperature (T), and the vegetation specific minimum resistance (R_{smin}) according to the standard parameterization of Wesely (1989). While the factors controlling stomatal resistance to H_2O transfer, and the applicability of H_2O resistance schemes to other gases, are well established, much less is known about the cuticular resistance (R_w) of NH_3. Previous studies have shown that cuticular adsorption of NH_3 depends on the chemical characteristics of the cuticle and surface water layers (Flechard et al., 1999). Studies [(Fowler et al. (1998), Jones et al. (2007)] have also shown an increase in R_w with increasing NH_3 concentration in air as the cuticle becomes saturated. This has important implications for the work presented here, as very high concentrations of NH_3 are expected near animal production facilities. In this case, we use the concentration-dependent R_w parameterization of Jones et al. (2007) for *C. vulgaris*. While it is recognized that this parameterization may not be generally applicable, specific parameterizations for vegetation types across eastern North Carolina have not yet been developed.

The in-canopy aerodynamic (turbulent) resistance (R_{ac}) is calculated according Zhang et al. (2003) as a function of u_*, single-sided leaf area index (LAI), and the vegetation specific minimum in-canopy aerodynamic resistance (R_{acmin}). The additional boundary layer resistance (R_{bg}) at the ground is calculated according to Schuepp (1977) and applied similarly to Nemitz et al. (2000). The sum of R_{ac} and R_{bg} establishes the total ground resistance (R_g)

In the case of NH_3, leaves may act as a source or sink depending on the ratio of the ambient concentration to the stomatal compensation point (χ_s) (Farquhar et al., 1980; Husted and Schjoerring, 1995). χ_s is a function of temperature and the apoplastic concentrations of NH_4^+ and H^+ (Nemitz et al., 2000). The leaf emission potential $\Gamma_s = NH_4^+/H^+$ has been shown to vary widely as a function of plant and soil nitrogen status (Schjoerring et al., 1998; Sutton et al. 1997; Flechard and Fowler, 1998). Similar to the leaf apoplast solution, the equilibrium between gaseous NH_3 and NH_4^+ in the soil pore space and fresh/salt water solution establishes a soil/water compensation point, referred to here as χ_g (Dawson, 1977; Nemitz, 2001) with a corresponding specification of Γ_g. For example, fertilized soils, which have a large value of Γ_g, will be a net source of NH_3 in the model, while forest soils or open water, which conversely have small values of Γ_g, may oscillate between source and sink throughout the year. Thus, the model takes into account bidirectional NH_3 exchange with vegetation as well as soil and fresh/salt water. Since direct measurements of apoplast and water/soil solution chemistry are not yet available for all of the surface types within the model domain, appropriate values have been selected from peer reviewed literature (e.g., references above; Walker et al., 2006; Walker et al.,

2008; Cooter et al., 2010). Gamma values for individual land use categories are held constant throughout the year.

Air-surface exchange fluxes are calculated by land use according to the 2001 National Land Cover Data imagery classification, which contains 21 land use classes at 30m horizontal resolution (NLCD, 2001). Land use specific inputs include Γ_s, Γ_g, LAI, R_{acmin}, and R_{smin} (Appendix A, Table 12) . The model is driven with hourly meteorological data from the nearest NC AGNet station (NCSCO, 2007), including wind speed, standard deviation of wind direction, air temperature, and soil temperature.

2.2 MODEL IMPLEMENTATION

Geographic Information System (GIS) software and custom built components are used to calculate and analyze the atmospheric concentration field within the SEADE model. The GIS is used to create, maintain and store the emissions inventory and in the analysis and visualization of model outputs. Custom algorithms compute concentration fields and include ArcInfo scripts and C code executed in batch mode. Because of computational concerns and a potential future need for supercomputer compatibility, the concentration field model is developed with support for cross-platform compilation.

The model domain is controlled by scripts that use both the CAFO's database and a predefined lattice distance. Export functions within the scripts create the input files required by the atmospheric concentration model. These scripts manage the spatial boundaries and verify that the output resolution and facility locations are based on the select coverage area. When a non-rectangular model domain is specified, lattice points that fall outside the coverage area are removed in order to reduce the computational time of the atmospheric concentration model.

The SEADE modeling system is implemented by first calculating facility scale emissions, followed by calculation of ambient NH_3 concentrations, followed by calculation of net air-surface exchange fluxes. As described above, a concentration is predicted at each point within the 100m by 100m lattice, producing a distribution of $N = Z$ concentration estimates where Z equals the total number of animal production facilities within the model domain. To produce smooth concentration fields, the maximum concentration at each point is retained and the source farm and distance are recorded. Next, the concentration field is converted to a raster data model and the air-surface exchange rate is calculated at each cell by applying land use parameters, meteorological data, and concentrations following the framework described in Section 2.1.3.

To calculate air-surface exchange rates, hourly meteorological data for the period of interest are reduced to an average diurnal profile. The diurnal profile of meteorological parameters is then used to generate a diurnal profile of air-surface exchange at each prediction point. Hourly estimates are then aggregated to produce a representative daily flux at each model prediction point, which is then scaled up to a seasonal value.

3. RESULTS

3.1 MODEL CALIBRATION

3.1.1 Atmospheric Concentrations

Measured NH_3 decreased exponentially with distance from the nearest animal facility during all seasons (Figure 2). The magnitude of observed concentrations varies by season with summer concentrations the greatest, then spring, fall, and winter. In general, winter concentrations were half of summer and spring and fall around 80% of summer. At distances > 2 km, average seasonal concentrations showed much lower variability (Figure 3) than concentrations near facilities.

Figure 2: The yearly average NH_3 concentration measured during the Lizzie and CAMNet studies (Walker, *et al.*, 2000b). Concentrations decrease exponentially with distance from the nearest animal facility.

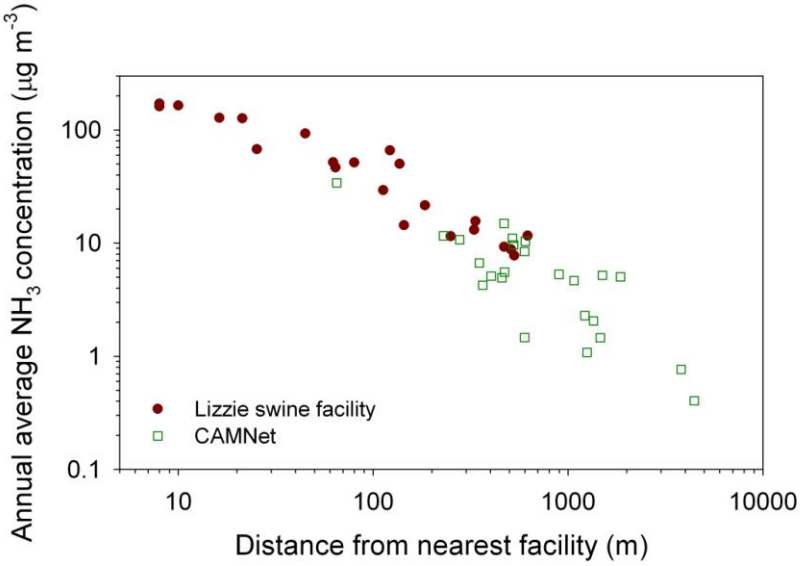

Figure 3: Yearly average NH_3 concentration in air for each of the 23 CAMNet monitoring stations. The average seasonal minimum and maximums are show as error bars.

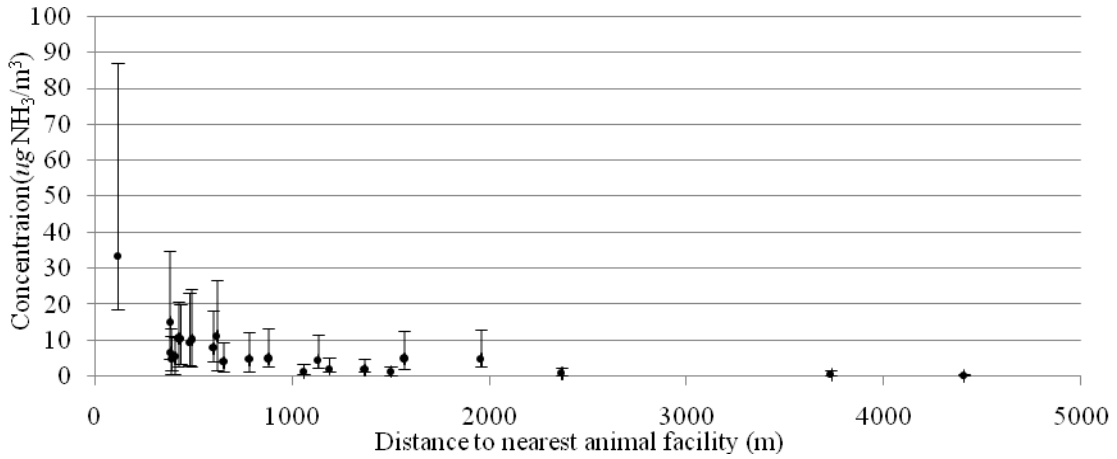

Multiple linear regression was used to test the significance of different independent variables potentially important to modeling the variability of the observed NH_3 air concentration. Variables included the distance to the closest facility, total estimated yearly emissions from the closest facility, the number of barns observed at the closest facility and the upwind direction to the closest facility. The variables were tested for each season against log transformed ammonia concentrations. The regression analysis indicates that the distance to the closest facility is significant during all seasons ($\alpha = 0.05$). The analysis also indicates that the additional variables do not provide significant added strength in predicting the concentration of NH_3 in air and are therefore excluded from the concentration model (Table 1).

Table 1: Variables tested and their significance in the parameterization of the concentration model. ($\alpha = 0.05$). Significant values are highlighted in bold.

Parameter	Spring	Summer	Fall	Winter
closest facility	**< 0.001**	**< 0.001**	**< 0.001**	**< 0.001**
total yearly emission	0.49	0.52	0.69	0.25
barns at closest facility	0.52	0.40	0.49	0.24
upwind direction	0.40	0.19	0.08	0.55

The regression analysis indicates that the strength of the model remains consistent between seasons with correlations ranging from 0.67 in the fall to 0.74 in the spring and winter (Figure 4). The intercepts support the expected influence of temperature on the NH_3 concentration with, summer being the highest, followed by similar spring and fall, then winter having the lowest

average concentration. This pattern is driven by the exponential relationship between temperature and NH_3 emissions from animal manure.

Figure 4: Linear model illustrating the concentration of ammonia in air versus the distance to the nearest animal facility for each of the modeled seasons.

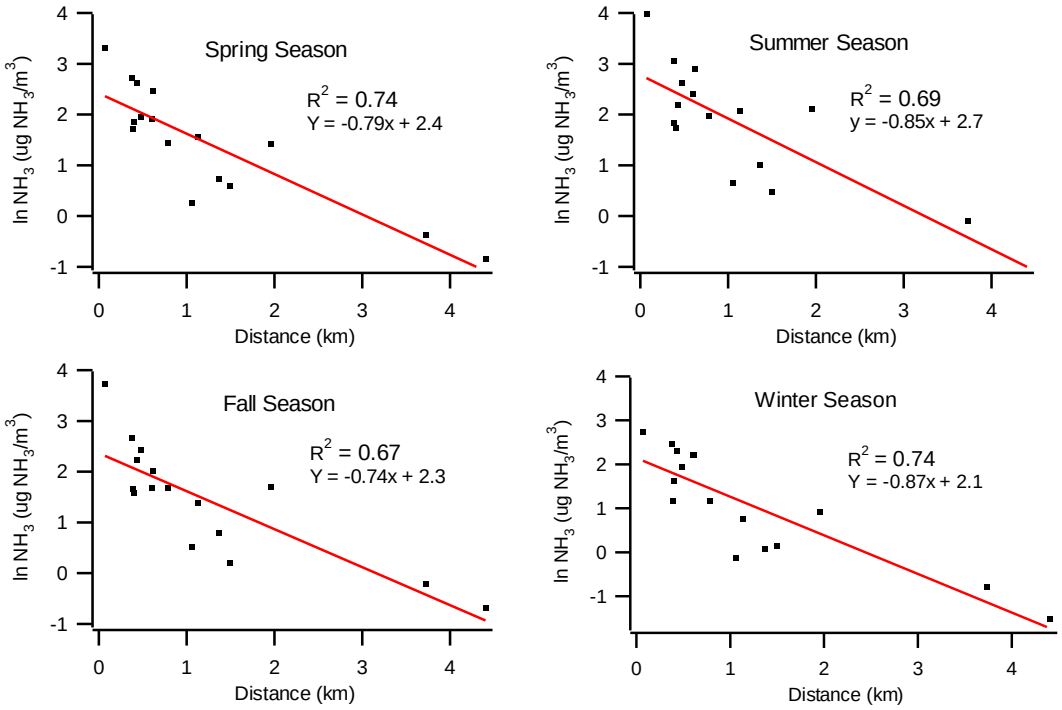

Based on the results of the regression analysis, models I and II were calibrated using a nonlinear regression model of the form $y = aX^k$ as described in Section 2.1.2.1. The nonlinear regression procedure (SAS Proc NLIN) estimates the parameters using a nonlinear least squares procedure that minimizes the weighted residual sum of squares. The regression parameters (Table 2) were estimated using seasonally averaged NH_3 concentrations from the 16 calibration sites. The calibration procedure revealed considerable variability between the seasonal decay exponent *k* with k_{spring}= -0.65, k_{summer}= -0.81 , k_{fall}= -0.87, and k_{winter}=.-0.53. The seasonal coefficient *a* derived for Model III was also determined using the same nonlinear least squares analysis, yielding values of 437, 1684, 1710, and 159 for spring, summer, fall, and winter, respectively.

Table 2: Various forms of the distance-decay, shifted power law function used to predict the average seasonal surface concentration of ammonia (NH_3) in air ($\mu g/m^3$).

	spring	summer	fall	winter
Model I	$NH_3 = aX^{-0.75}$	$NH_3 = aX^{-0.75}$	$NH_3 = aX^{-0.75}$	$NH_3 = aX^{-0.75}$
Model II	$NH_3 = aX^{-0.65}$	$NH_3 = aX^{-0.81}$	$NH_3 = aX^{-0.87}$	$NH_3 = aX^{-0.53}$
Model III	$NH_3 = 437X^{-0.65}$	$NH_3 = 1684X^{-0.81}$	$NH_3 = 1710X^{-0.87}$	$NH_3 = 159X^{-0.53}$

3.1.2 Ammonia Air-Surface Exchange Model

Air temperatures followed expected trends ranging from daytime highs in the summer of 30°C (86°F) to lows of 20°C (68°F). In the winter, daytime highs averaged 18 °C (64°F) while lows averaged around 4°C (39°F) (Figure 5). The average diurnal soil temperatures for each season follow a pattern similar to air temperature, however, daytime highs peak a few hours later and exhibit a smaller daily range. This pattern is driven by the radiant transfer of heat through the soil profile and the buffering capacity of moisture in the soil.

Figure 5: Average 24-hour profile for daytime air temperate and soil moisture for each of the 4 seasons modeled. Air temperature is shown as a solid line, soil moisture as a dotted line.

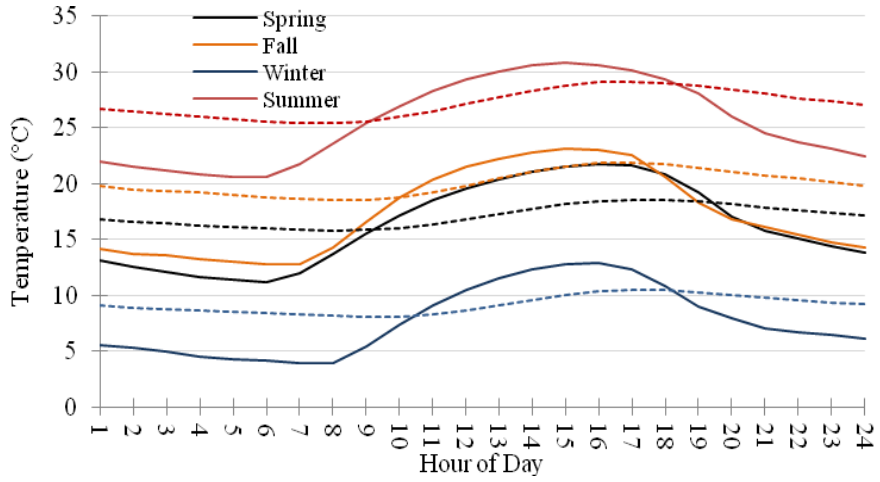

Wind direction, standard deviation of wind direction (Yamartino, 1984), wind speed, and corresponding atmospheric resistances (R_a, R_b, R_g) were divided into seasons and averaged by hour of day (Figure 6). Seasonally, wind speeds were greater in the spring and winter and lower in the summer and fall. Wind speeds increase after sunrise and peak in the early afternoon, following the diurnal pattern of surface heating. Generally, as wind speeds increase during the day so does the standard deviation of wind direction, reflecting greater turbulent mixing during unstable periods. The atmospheric resistances follow an inverse pattern, with higher values corresponding to low wind speeds and reduced turbulent mixing at night, and lower values

during the day. Primary wind direction throughout the year and between all seasons averaged around 170 degrees or essentially from the South-Southeast.

Figure 6: Average seasonal 24-hour profile wind speed used in the air-surface exchange model.

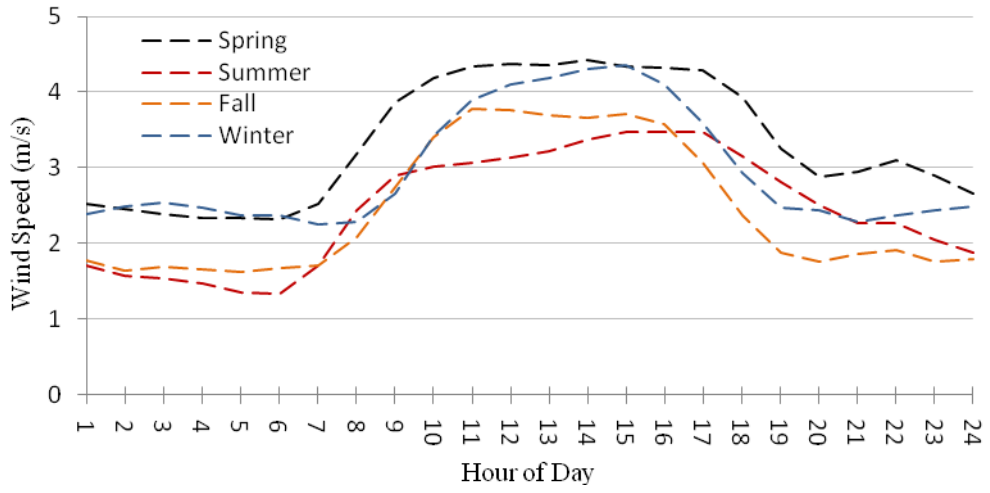

3.2 MODEL VALIDATION

3.2.1 Emissions Inventory

For each record in the emission inventory there is both a facility location (e.g. latitude, longitude) and a number for the permitted animals at that location. To validate the spatial locations, the animal operations were overlaid on the 2006 National Areal Imagery Program (NAIP) true color, orthorectified imagery. A GIS was used to overlay registered facilities with the aerial imagery and to visually observe any discrepancies. Because the CAFO permits are issued per facility, it was common to find multiple emission sources (i.e. lagoons, poultry houses, or spray fields) permitted as a single location. By using the imagery as a spatial reference, it was possible to visually validate the location of the permitted location. When a permitted facility was visually confirmed to consist of a single emission source and its location did not overlay with the emissions source (e.g. over a forest instead of the lagoon) it was moved to the proper location accordingly. When a single animal facility was used to represent multiple emission sources, the facility was split into multiple locations where each new location represented a fraction of the total number of animals permitted for that site.

The number of animals in the emissions inventory was validated with the county-scale animal activity data reported by the North Carolina Department of Agriculture and Consumer Services (NCDACS). To cross-check the data, the emissions inventory was aggregated by county and compared to the county-level statistics. Because county-level statistics from NCDACS are not developed from permitting requirements, this approach provides an independent evaluation of the NCDWQ facility scale database.

Table 3: Comparison between the number of swine reported by the NCDA&CS and that of the CAFO's-based emissions inventory. The top 8 swine producing counties are shown.

County	Emissions Inventory	NCDACS	Difference (%)
Duplin	2,285,586	2,167,000	5.2
Sampson	2,021,993	2,025,000	-0.1
Bladen	841,664	815,000	3.2
Wayne	514,049	515,000	-0.2
Robeson	274,410	353,000	-28.6
Green	431,428	350,000	18.9
Lenoir	293,863	312,000	-6.2
Columbus	240,610	244,000	-1.4
Pender	262,124	237,000	9.6

The CAFO's database requires permits for animal feedlots on liquid waste systems. As such, it does not include the vast majority of broiler, layer and turkey facilities in the state. The poultry included in the emissions inventory includes 25 facilities permitted for 5.9 million layers and 1 million non-laying pullets. According to NCDA&CS, in 2006 there were 750 million broilers produced, 20 million on-farm layers, and 37.5 million turkeys produced. Because facilities with dry-litter systems do not require a CAFO permit, the emissions inventory lacks 100% of the turkey facilities, 70% of layers, and virtually 100% of broilers and pullets, or an estimated 800 million birds across the state. County-level statistics are available from NCDA&CS and when mapped illustrate the main production regions (Figure 7). Based on this data it is roughly estimated that there could be as many as 350 million poultry and turkey within the study area that are unaccounted for in the emissions inventory.

Figure 7: Number of Broilers produced per county as reported by the North Carolina Department of Agriculture and Consumer Services (NCDA&CS, 2006).

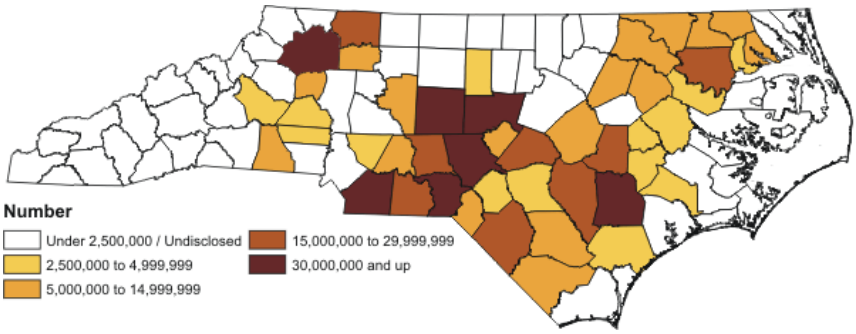

Comparing the total emissions from the CAFO-based emissions inventory with the independently collected 2007 animal numbers from the North Carolina Department of Agriculture Statistics (NCDAS) service provides an estimate of total basin-wide NH_3 swine emission within 6 percent of the SEADE emissions inventory. The SEADE emission inventory estimates a total yearly emission of 57.3 million kg while the NCDAAS -based estimate totaled 54.0 million kg of NH_3. The total NH_3 emission estimate for swine was calculated by multiplying the total swine reported by NCDAS by the fraction of the swine-types found within the basin (based on the CAFO's database), multiplied by the emission factor for that swine type (Section 2.1.2.2). A similar approach was used to calculate total yearly NH_3 emissions in the SEADE inventory and so allows for an unbiased cross-comparison between data sets.

Underestimation of SEADE emissions due to exclusion of poultry and cattle may be assessed by comparing SEADE total emissions to total emissions from swine, turkeys, broilers chickens, layer chickens, and beef and dairy cattle develop from NCDAS county level animal activity data and the emissions factors cited (Table 4). In 2007, the North Carolina poultry inventory included 863 million head; 11.0 million layers, 11.3 million pullets, 781.4 million broilers, and 60.0 million turkeys. Based on the county-level poultry data from NCDAS it is estimated that 31 percent, or approximately 267 million birds, fall within the study area. Because county boundaries do not coincide with the river basin boundaries, the number of animals within a county was partitioned based on the fraction of the county within the study area. For example, 56 percent of Randolph County falls within the study area and within all of Randolph County there are a reported 47 million broilers, 26.3 million that would be included in the emission calculation. To calculate the net NH_3 emission for poultry, the total number of birds was divided by the number of flocks per year (5.75 for broilers, 3.5 for turkeys, 5.75 for chickens, Walker et al., 2000b) then multiplied by the yearly emission factor for the poultry type.

Table 4: Comparison between the total yearly NH_3 emissions as calculated within SEADE and as calculated from the county-level production numbers reported by the North Carolina Department of Agriculture Statistics (NCDAS) Service.

SEADE	**NCDA Agricultural Statistics**					
Swine *(kg x 10^6)*	Swine *(kg x 10^6)*	Turkey *(kg x 10^6)*	Chickens *(kg x 10^6)*	Broilers *(kg x 10^6)*	Cattle *(kg x 10^6)*	Total *(kg x 10^6)*
57.3	54	7	0.24	6.8	9.2	77.24

Total SEADE emissions represent 75% of total emissions from all animal categories derived from NCDAS animal activity data.

3.2.2 Ammonia Concentration Model

Aerial imagery taken during the study period was used to locate and identify all animal facilities within a 5km radius of a CAMNet site. Because the CAFO's database does not contain facilities under dry waste systems, (e.g. poultry) it was particularly important to identify and mark these locations so as to capture all emission sources close to a CAMNet site used in model calibration. Additionally, the exact locations of swine facilities were identified and moved or split into multiple sources when the areal imagery provided sufficient visual evidence. The identification of the closest animal facility within that 5km buffer was vital to the calibration procedure due to the sensitivity of the model to the distance from the nearest source.

Seasonal performance metrics for the three models are given in Table 5. As described above, Model I was validated against the complete set of CAMNet sites. Mean bias ranged from -1.49 $\mu g\ NH_3\ m^{-3}$ in the winter to 2.1 $\mu g\ NH_3\ m^{-3}$ in the summer, indicating that the model tended to overestimate during warm months and underestimate during cold months. Normalized mean error of Model I was on the order of 50%, though slightly lower in the spring (36%). Monthly regression plots are shown in

Figure 8. The predictive error is shown as the vertical offset from the plotted 1:1 red line. The model was evaluated by observing both the slope and intersect of a best-fit line through the data (Figures 8,9,10). Slopes greater than 1 indicate the model is under predicting at low concentrations and over predicting at higher concentrations. Slopes less than 1 indicate the opposite. Confidence intervals were graphed to display the variance of the modeled results and help evaluate model significance. For Model I, regression plots revealed strong correlation between model and observations and follow a pattern of model overestimation at low concentrations and underestimation at high concentrations.

Table 5: Seasonal model performance metrics: mean bias (MB, µg m^{-3}), normalized mean bias (NMB, %), root mean square error (RMSE, µg m^{-3}), normalized mean error (NME, %), and correlation coefficient (r).

		MB	NMB	RMSE	NME	R
Model I	Spring	-0.61	-10.32	2.70	35.72	0.82
	Summer	2.12	27.98	4.64	47.28	0.71
	Fall	1.44	27.05	3.17	48.21	0.71
	Winter	-1.49	-34.29	2.75	49.23	0.82
Model II	Spring	5.16	90.08	6.08	90.08	0.79
	Summer	-11.02	-9.50	4.27	47.35	0.72
	Fall	-1.97	-37.34	3.29	44.52	0.73
	Winter	8.30	185.97	9.38	185.97	0.74
Model III	Spring	0.07	1.21	2.99	42.02	0.78
	Summer	0.20	2.56	4.63	49.65	0.64
	Fall	0.18	3.51	2.49	36.98	0.73
	Winter	0.15	3.37	2.74	54.68	0.79

Figure 8: Predicted concentration versus observed for Model I. Best fit line shown in black with 95% confidence intervals.

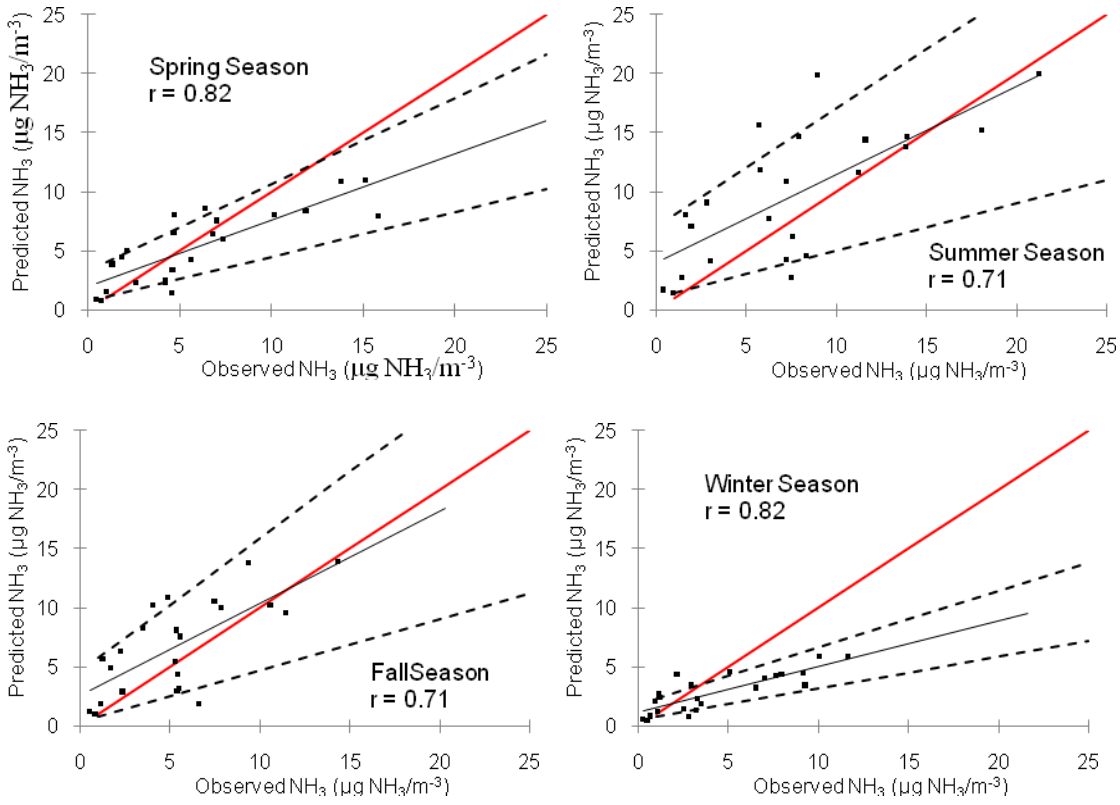

Figure 9: Predicted concentration versus observed for Model II. Best fit line shown in black with 95% confidence intervals.

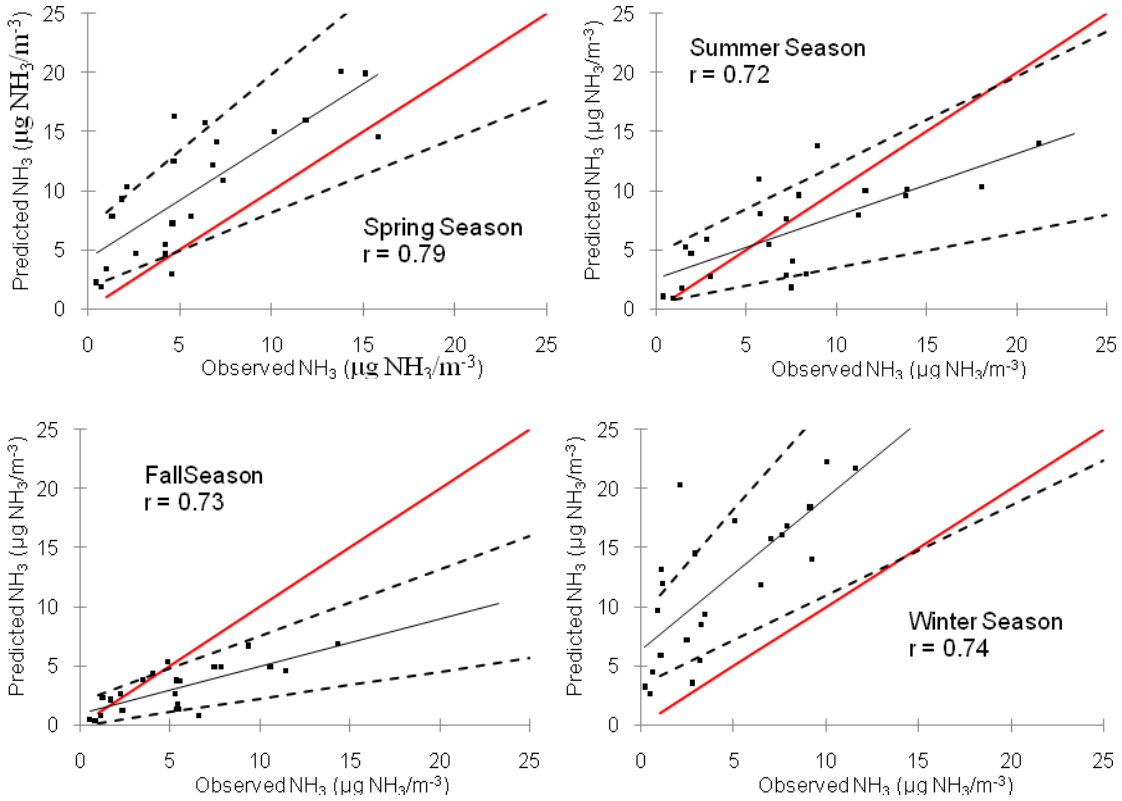

Model II (Table 5,
Figure 9) was validated against the eight randomly selected CAMNet validation sites. Mean bias ranged from -11.02 µg NH_3 m^{-3} in the summer to 8.3 µg NH_3 m^{-3} in the winter, indicating that the model tended to underestimate during warm months and overestimate during cold months. Unlike Model I, the normalized mean error varied significantly between seasons. In the winter, normalized mean error was over 3.5 times as great as predicted by Model I. The overall seasonal accuracy of Model II, as determined by the root mean square error, showed fall predictions as the most accurate (3.3), followed by summer (4.3), spring (6.1), and then winter (9.3).

Figure 10: Predicted concentration versus observed for Model III. Best fit line shown in black with 95% confidence intervals.

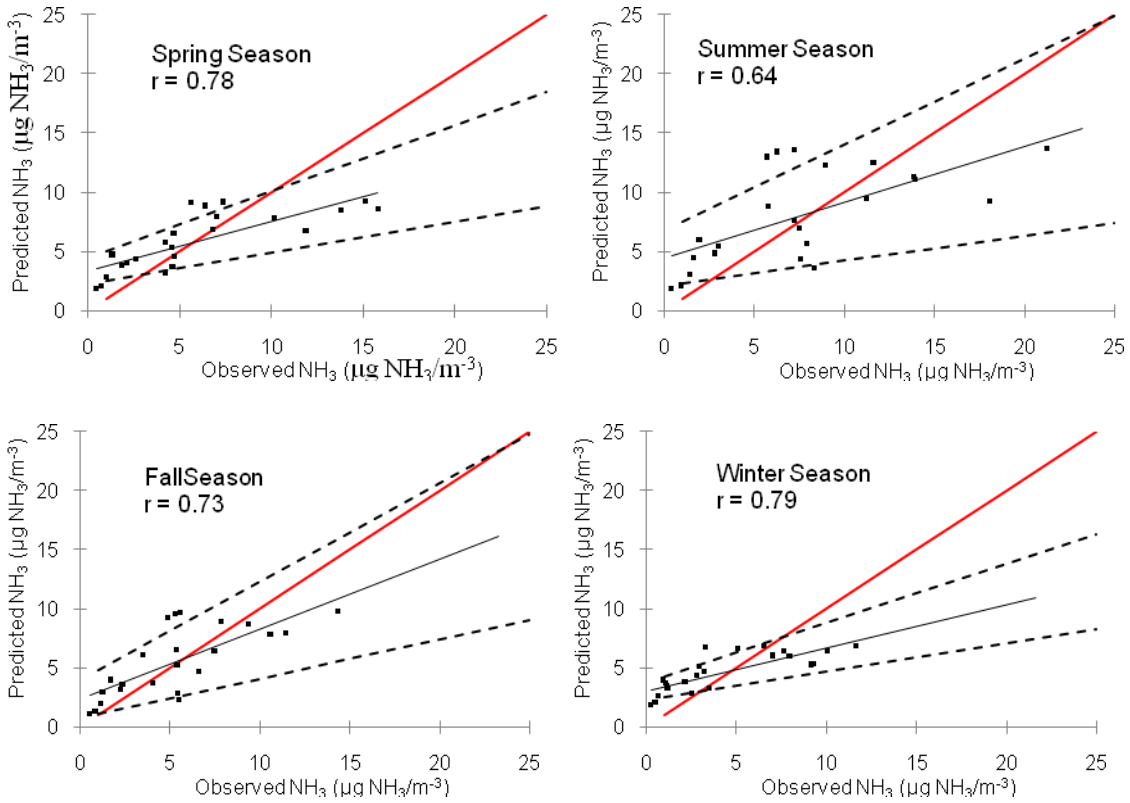

Model III (Table 5,

Figure 10) was also validated against the eight randomly selected CAMNet validation sites. Mean bias showed little variation between seasons and averaged around 0.16 µg NH_3/m^{-3} annually. Out of the three concentration models tested, Model III had the overall lowest mean bias. In the case of Model III, the low mean bias is a result of the over predictions at greater distances negating the under prediction at closer distances, not a better overall model accuracy. Model III was entirely parameterized using CAMNet data, and as such the overall low mean bias is expected. The normalized mean error for Model III is similar to Model I. The overall seasonal accuracy of Model III, as determined by the root mean square error, showed fall predictions as the most accurate (2.5), followed by winter (2.7), spring (2.9), and then summer (4.6).

In general, Model I over predicts at lower concentrations (< 3ug/m^3) and under predicts at higher concentrations in the spring, summer, and fall. In winter, Model I consistently under predicts concentrations, most likely due to the static seasonal decay constant *k*. This may reflect the influence of emissions (poultry) not captured in the SEADE inventory that display less seasonal variability than swine emissions, i.e., the lack of poultry emissions in our model may be most evident during the winter. The largest range in prediction error occurs in the summer when observed concentrations are highest. During summer and fall, the best-fit trend line was statistically similar ($\alpha = 0.05$) to the observed data (e.g. the 95% confidence interval included a slope of 1, $LCI \leq 1 \leq UCI$). During all seasons the intercept of the best-fit line is statistically significant; however, the range of the 95% confidence interval never includes the expected intercept of 0 for any season. The seasonal intercepts for Model I were; spring = 1.9 μg NH_3 m^{-3}, summer = 4.0 μg NH_3 m^{-3}, fall = 2.6 μg NH_3 m^{-3} , and winter = 1.1 μg NH_3 m^{-3}, which are higher than the lowest seasonal average concentrations (0.54,0.38, 0.45, and 0.17 μg NH_3 m^{-3} in spring, summer, fall, and winter, respectively) observed at a remote site (site P15, Figure 11) uninfluenced by emissions from animal facilities. However, at the watershed scale, the minimum predicted concentrations agree closely with seasonal average concentrations at this remote site (Figure 11).

Figure 11: Comparison of seasonal mean observed concentrations (1 standard deviation) at remote CAMNet site P15 to seasonal minimum predicted concentrations in the Neuse and Cape Fear River basins.

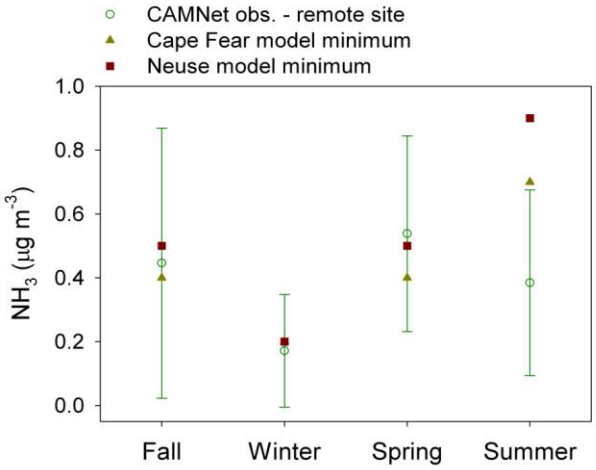

Model II produced a range of seasonally inconsistent prediction errors. In the spring and winter the model over predicted concentrations at all but 2 sites. In the summer and fall the model over predicted lower observed concentrations while under predicting higher values. The slope of the regression line is within the 95% confidence interval in the spring and winter ($\alpha = 0.05$),

however, in the summer and fall the trend line is not statistically similar. Model II is most accurate during the summer, followed by the fall, spring, and winter. Like Model I, the intercept for all seasons is statistically significant, however, unlike model I the magnitude and seasonal pattern of the intercept does not follow observed values. The seasonal intercepts for Model II were; spring = 4.0 μg NH_3/m^{-3}, summer = 2.6 μg NH_3/m^{-3}, fall = 1.3 μg NH_3/m^{-3} , and winter = 9.0 μg NH_3/m^{-3}.

In general, Model III predicts concentrations best between the range of 5 and 10 μg NH_3/m^{-3}. Outside this range however, the model consistently overestimates concentrations at lower values and under predicts sites at higher concentrations. The correlations between model predictions and observed values between seasons are similar to Models I and II, however, no statistically significant trend is observed with Model III. The seasonal intercepts for Model III were; spring = 3.4 μg NH_3/m^{-3}, summer = 4.5 μg NH_3/m^{-3}, fall = 1.0 μg NH_3/m^{-3} , and winter = 6.3 μg NH_3/m^{-3}.

Results from the validation procedure indicate that Model I most closely predicts the observed NH_3 concentrations. Although the prediction errors are slightly higher for Model I, the validation includes the entire 24 stations as opposed to the subset of 8 used for Model's II and III. Model I generally overpredicted concentrations at points located greater than 3km away from the nearest animal facility, however the predictions followed observed seasonal trends unlike Models II and III. Model I showed the greatest difficulty predicting concentrations in the winter. However, because of the lower concentrations observed in the winter the overall prediction error remained small when compared to the other seasons.

The results from the calibration and validation procedure indicate that a model that scales emissions based on facility size and that applies a static decay constant provides reasonably accurate predictions of air concentration over a range of spatial and temporal scales (Table 5). When comparing the average error between primary facility type (i.e. swine versus poultry) by splitting the dataset according to type of nearest facility, the mean errors are statistically similar (swine $\bar{\varepsilon}$ =0.3 $\mu g\ NH_3\ m^{-3}$, poultry $\bar{\varepsilon}$ = 0.5 $\mu g\ NH_3\ m^{-3}$) (α = 0.05), while the difference between the range of predictions varies by over 3 $\mu g\ NH_3\ m^{-3}$ (swine = 14.0 $\mu g\ NH_3\ m^{-3}$, poultry = 17.7 $\mu g\ NH_3\ m^{-3}$). The inability to classify the type of poultry facility from aerial photography and the resulting implementation of a single yearly emission factor for all poultry types (i.e. layer, pullet, turkey, and broilers) likely contributes to the variability of prediction error observed around poultry facilities. A related source of error is the lack of publicly available spatial data that identifies the locations of poultry operations. Although we visually located poultry operations using aerial photography during the calibration and validation procedure, due to the vast resources and time required to manually locate, record, and archive the estimated 2500 poultry operations in this state, this was not performed for the entire Cape Fear and Neuse river basins. Modeling without a comprehensive emissions inventory is a potentially important source of error and likely results in a general under prediction of NH_3 concentration and deposition. Because of

the rapid decrease of NH_3 concentration with distance, the largest errors will occur in areas heavily populated with poultry and cattle. Thus, lack of information on these facilities is an important limitation of this modeling approach.

The results suggest that using the same decay constant for summer and fall models the decay of NH_3 reasonably well; however, for spring and winter the decay constant appears to be too large. By reducing the decay constant in the spring and fall the model will predict higher concentrations at distances further from facilities. A decay constant calibrated separately for each season would likely better characterize the decay of NH_3 with distance from a facility. Especially in winter, these results support the observed increase in wind speed and thus more rapid dispersion and decrease in concentration with downwind distance during these months.

The magnitude of prediction error is highly dependent on the distance to the nearest source and the size of the facility. This error pattern is expected due to the exponential form of the decay function and dependence of the initial scaling on facility size. At a distance of over 1.8 km the predictions fall to within 3 $\mu g\ NH_3\ m^{-3}$ of observed values. Additionally, the largest prediction errors occur in the summer and smallest in the winter primarily due to the temperature dependence of NH_3 emissions.

Figure 12: Relationship between the distance to the nearest NH_3 emission source and the magnitude of the prediction error.

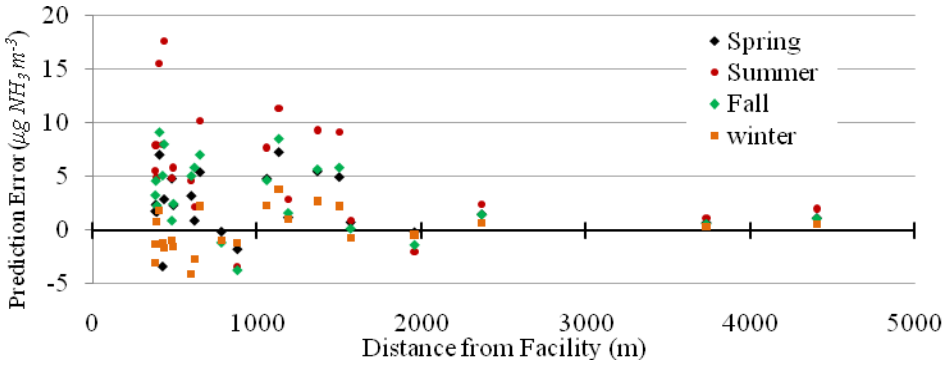

The initial scaling factor *a* (equation 6) plays a critical role in accurately predicting concentrations at locations less than 500 meters away. For example, at a 5000 animal feeder-to-finish swine operation the model predicts that within the first 20 meters concentrations will drop on average 100 $\mu g\ NH_3\ m^{-3}$ per linear meter away from the source in the summer. At approximately 100 meters the same facility is modeled to decrease 1 $\mu g\ NH_3\ m^{-3}$ for ever linear meter away from the facility location. Because the decay constant is held constant between seasons, changes in the scaling coefficient a_j result in a concentration increase directly proportional to the increase in a_j. For instance, the model predicts for a 2500 animal swine

operation in the summer a concentration of 30 $\mu g\ NH_3\ m^{-3}$ at 100 m. At the same distance but for a 5000 animal facility the model predicts 60 $\mu g\ NH_3\ m^{-,3}$, two times the facility with half the animals. Because of the scaling coefficient and because the model only records the maximum concentration at a location, the concentration field in areas densely populated with animal facilities is primarily determined by the largest facilities. In these areas, accurately locating the largest facilities is of critical importance in modeling the concentration field.

Given the large spatial and temporal variability of observed NH_3 concentrations in areas densely populated with animal production facilities, the accuracy of the three models is limited by a lack of observational data from which the models are constructed. Model II should be the most physically representative of the three models tested, because emissions (coefficient a_j) are modeled as a function of facility type, size, and season, and dispersion characteristics (decay constant, coefficient B) may vary by season. Phase II of the SEADE model development will examine the performance of the models using data from an additional 25 sites. In this forthcoming analysis, we will also examine the usefulness of including the Lizzie dataset (Walker *et al*., 2008), from which Model I was developed, in the construction and validation of Models II and III.

3.3 WATERSHED-SCALE CONCENTRATION DISTRIBUTIONS

The concentration model was run for both the Neuse and Cape Fear river basins and results mapped using a GIS (Figures 13 and 14). The concentrations were drawn using a stretched standard deviation to help visually illustrate the dependence of concentration on season, distance to nearest animal facility, and overall size of the nearest facility. Without stretching the predicted concentrations, the map results in small, extremely localized areas of color, difficult to visualize at the watershed scale. This is important to note as it emphasizes the localized nature of the highest concentrations. As observed on the maps, the highest concentrations are found in the summer and directly adjacent to the largest facilities. Concentrations decay quickly as distances increases from a facility; however, very large facilities can dominate an area.

In both river basins the highest concentrations are found adjacent to large facilities and appear as larger sized ‘bulls-eyes’ on the maps. The emissions from these facilities dominate the area and thus control the models’ predicted concentration surrounding the facility. For example, in the Neuse there is a wean-to-feeder swine facility that is permitted for almost 26,000 animals. Although it is unlikely that the source of the emission occurs at a single location, it is still evident that, because of the large scaling coefficient, very large facilities dominate the concentrations in localized areas. In this case, even though there are other facilities in the area, within a 5km buffer around the facility the concentration field is determined by that single, large facility.

The average concentrations for the Neuse in the spring, summer, fall, and winter were 2.3, 3.8, 2.4, and 0.9 μg NH_3/m^{-3} respectively. In the Cape Fear the concentrations averaged 2.2, 3.6, 2.3, and 0.9 μg NH_3/m^{-3} respectively. During the summer, 90% of the area within the Cape Fear and Neuse river basins is predicted to average below 22 μg NH_3/m^{-3}, 50% of the area is predicted to average below 8 μg NH_3/m^{-3}. Seasonal minimum predicted concentrations compare well (Figure 11) with observations at clean sites that did not appear to be influenced by emissions from animal facilities (sites > 3.5 km from nearest facility in Figure 12). The low concentrations occur in areas with little animal production and the highest concentrations at locations directly adjacent to the largest permitted facility.

Figure 13: Average seasonal concentrations for the Neuse River Basin as predicted by Model I.

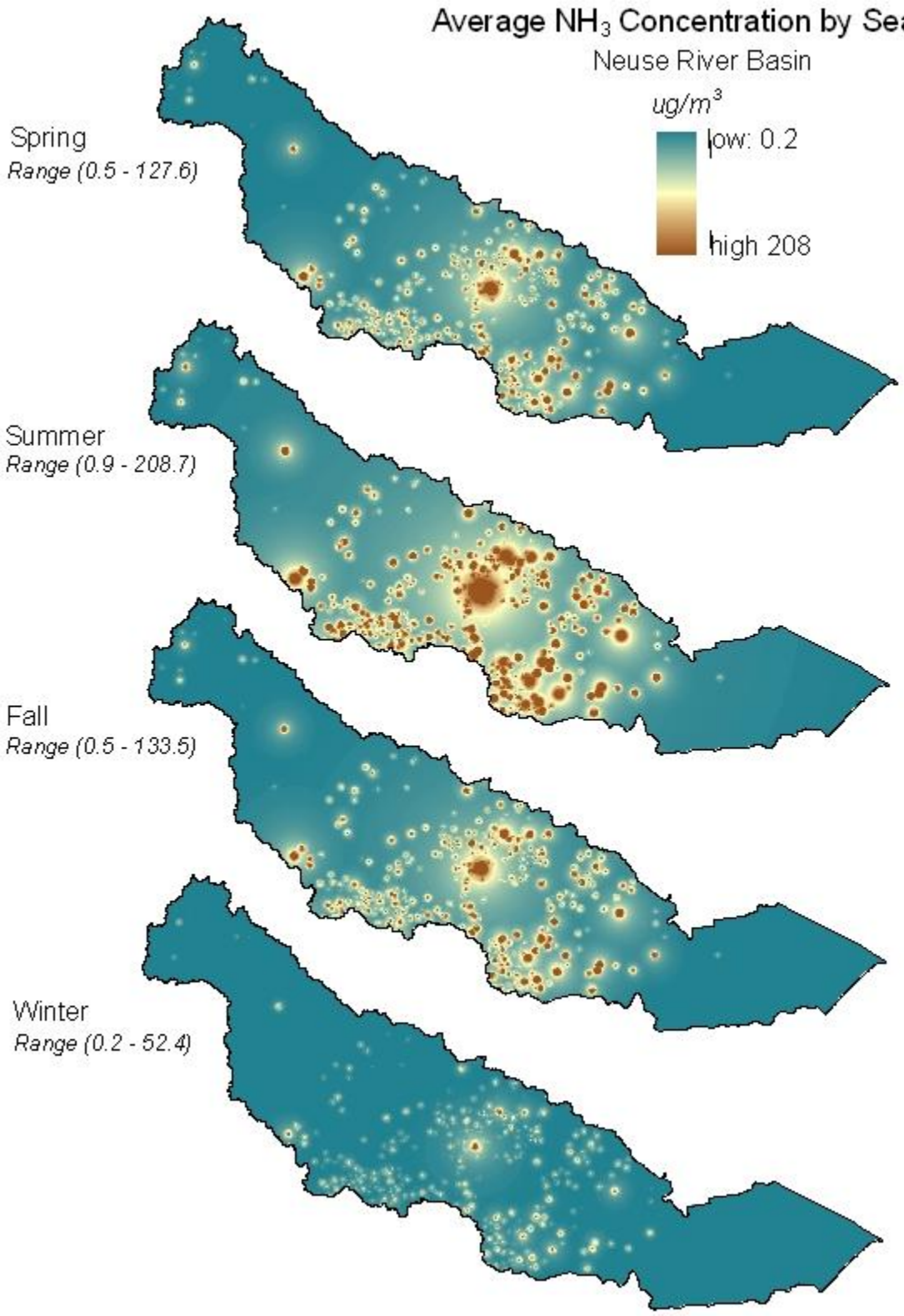

Figure 14: Average seasonal concentrations for the Cape Fear River Basin as predicted by Model I.

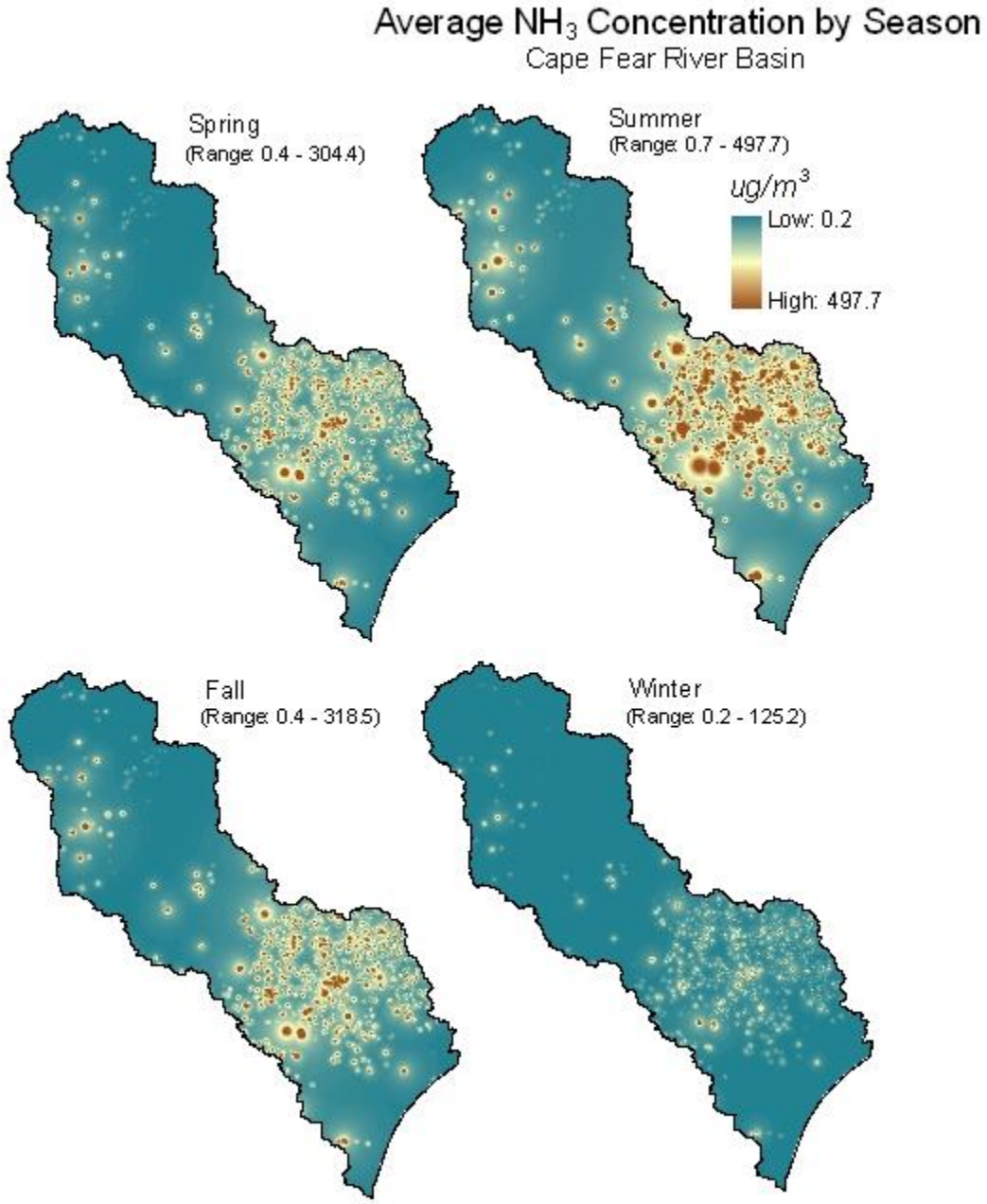

3.4 WATERSHED-SCALE DEPOSITION

Using a SAS™ routine developed to calculate NH_3 fluxes as describe in section 2.1.3, the total seasonal flux was calculated for each basin and for each season. The results were imported into a GIS as a 100m x 100m lattice and converted to raster format for display (Figures 16 and 17). Similar to the results of the concentration model, the maps were drawn using a stretched standard deviation so as to help visualize the results.

The largest total deposition rates occur directly adjacent to the largest facilities and rates decrease rapidly with distance from the facility. Due to the rapid decrease in NH_3 concentration with distance, the majority of deposition occurs within a relatively small area. Over 70 percent of the net NH_3 deposition occurs within 2.5 kilometers of an animal facility. This equates to 30 percent of the study area or 14 million kg of NH_3 deposited over 1.2 million hectares. Over 95 percent of the net NH_3 deposited occurs within 10.0 kilometers of an animal facility totaling 19.6 million kg over 3.1 million hectares (Figure 15). Average deposition decreases rapidly with distance following the pattern of air concentrations.

Figure 15: Deposition versus distance from nearest animal facility as predicted by SEADE.

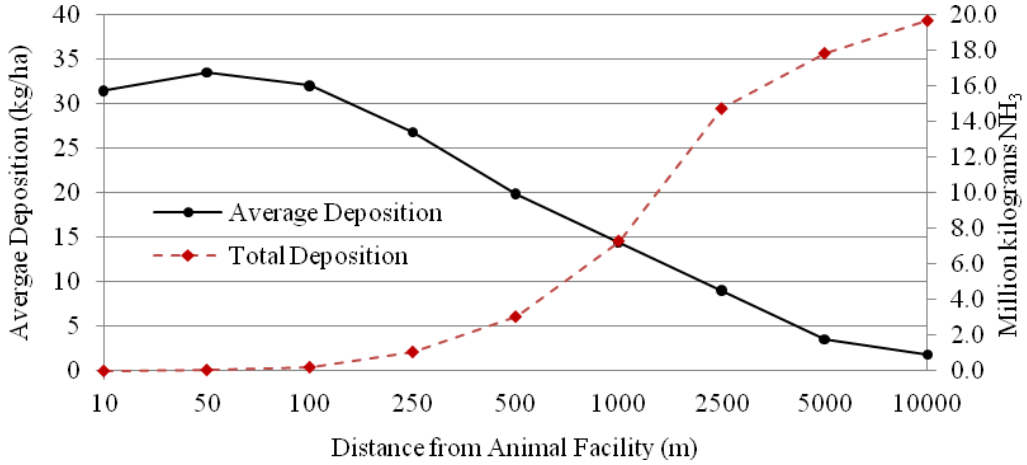

Land cover plays a critical role in watershed-scale deposition. NH_3 fluxes ranged from a maximum net emission of 6.5 kg ha^{-1} (cultivated crops) to a maximum net deposition of 170 kg ha^{-1}, both predicted during the summer season. This equates to a maximum average seasonal emission of 0.07 kg ha^{-1} day^{-1} and maximum average seasonal net deposition of 1.9 kg ha^{-1} day^{-1}. In the Neuse, net fluxes (deposition) averaged 1.2, 0.9, 1.2, and 0.6 kg ha^{-1} for the spring, summer, fall, and winter respectively. In the Cape Fear, net fluxes (deposition) averaged 1.3, 1.3, 1.4, and 0.6 kg ha^{-1} respectively. Like NH_3 concentrations, the areas subject to very large deposition totals occur over a very small fraction of the study area. For instance, approximately 10% of the study area averaged greater than 10.0 kg ha^{-1}; 50 percent of the study area averaged

less than 4.0 kg ha^{-1}. The highest net emission occurred in the summer over pasture land located in the extreme northwest corner of the Cape Fear basin, the furthest away from any animal facility and corresponding to the lowest air concentrations. Seasonally, the area of the Neuse and Cape Fear basins that yielded a net emission ranged from 21 percent in the summer to 13 percent of the basin in the winter, averaging 18 percent between all seasons.

Figure 16: Total seasonal ammonia flux for the Neuse river basin as predicted by the air-surface exchange model. Positive values indicate emission.

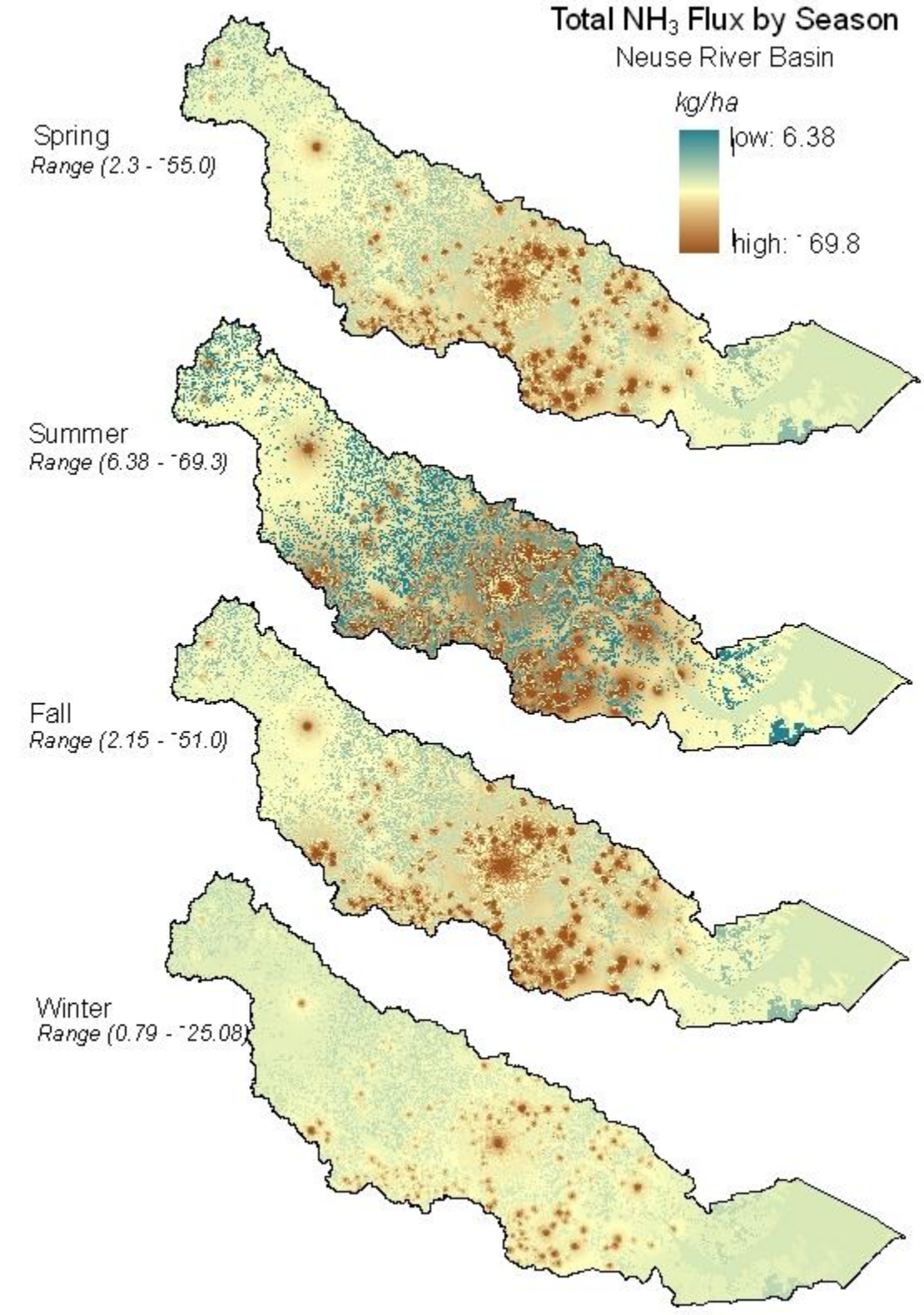

Figure 17: Total seasonal ammonia flux for the Cape Fear river basin as predicted by the air-surface exchange model. Positive values indicate emission.

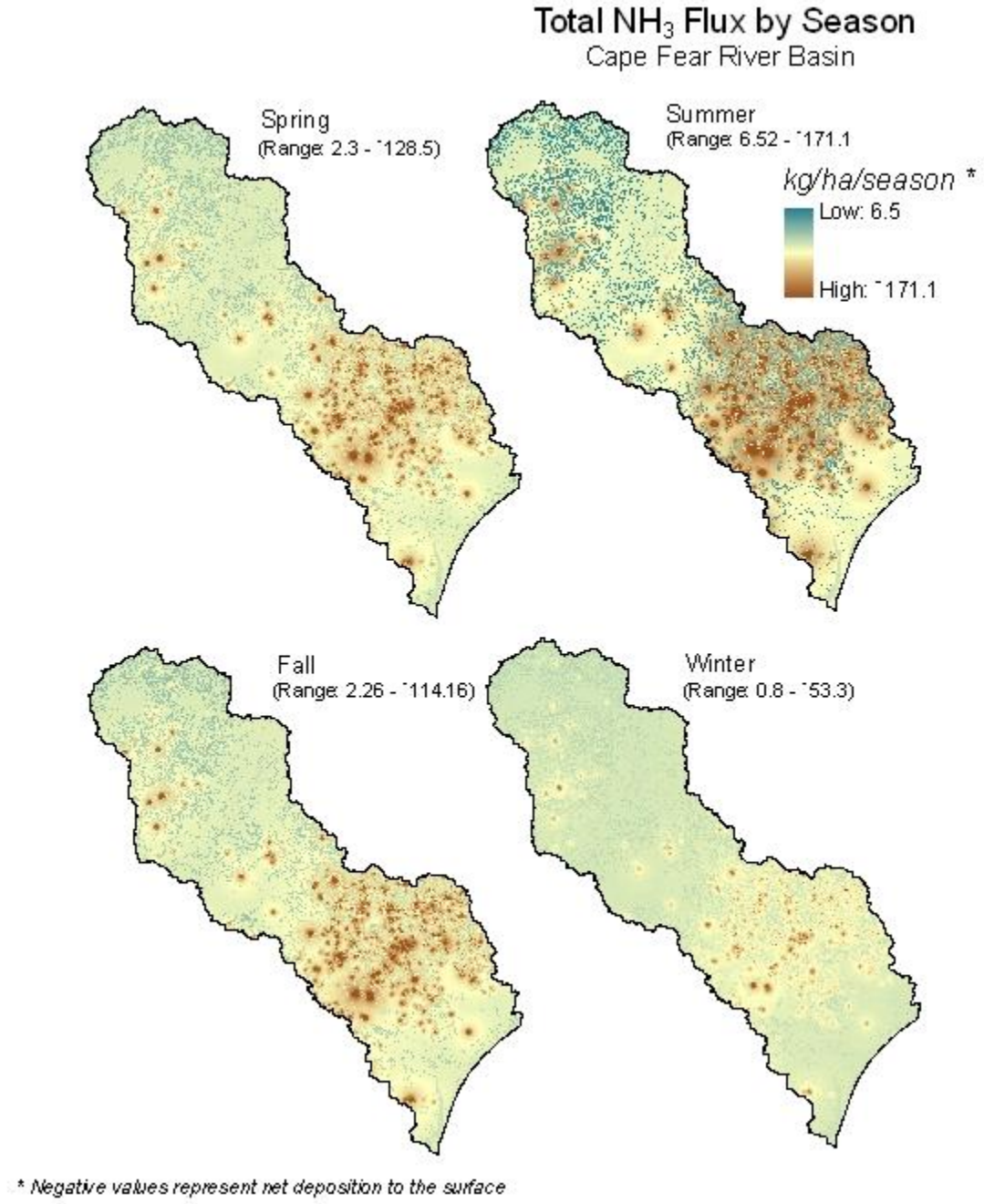

For the year, the air-surface exchange model predicted a net dry deposition totaling 20.6 million kg NH_3, 6.9 million kg within the Neuse and 13.6 million kg within the Cape Fear. Seasonal deposition totals were greatest in the fall, followed by spring, summer, and winter (Table 6). As a percent of total deposition, spring, summer, and fall were similar making up 29%, 27%, and 30% respectively. In winter, the percentage dropped to 14% of the total or 2.8 million kg dry NN_3.

Table 6: Total net dry deposition of NH_3 by season for the Neuse and Cape Fear river basins as predicted by the ammonia air-surface exchange model.

	Spring *(kg x 10^6)*	**Summer** *(kg x 10^6)*	**Fall** *(kg x 10^6)*	**Winter** *(kg x 10^6)*	**Total** *(kg x 10^6)*
Neuse	2.08	1.64	2.20	1.00	6.9
Cape Fear	3.86	3.98	4.04	1.80	13.7
TOTAL	5.94	5.62	6.24	2.80	20.6

On a county-by-county basis, 9 counties were modeled with a positive net NH_3 emission for the year. Three of the nine counties, Alamance, Guilford, and Carteret, have greater than 20% of their area within the Neuse or Cape Fear river basin. Of those three counties, Alamance exhibited the greatest total emission, ≈160,000 kg NH_3 for the year, an average of 1.48 kg NH_3 ha^{-1}. In contrast, 5 counties account for greater than half the total dry NH_3 in the study area with Sampson County receiving over 3.3 million kg of dry deposited NH_3 throughout the year (Figure 18). Although ranked 6^{th} in total deposition, Green County has the greatest per hectare average at -14.3 kg NH_3 ha^{-1}.

Figure 18: Average and total air-surface exchange of ammonia by county. Counties with less that 20% of their area within the study area are excluded from the maps.

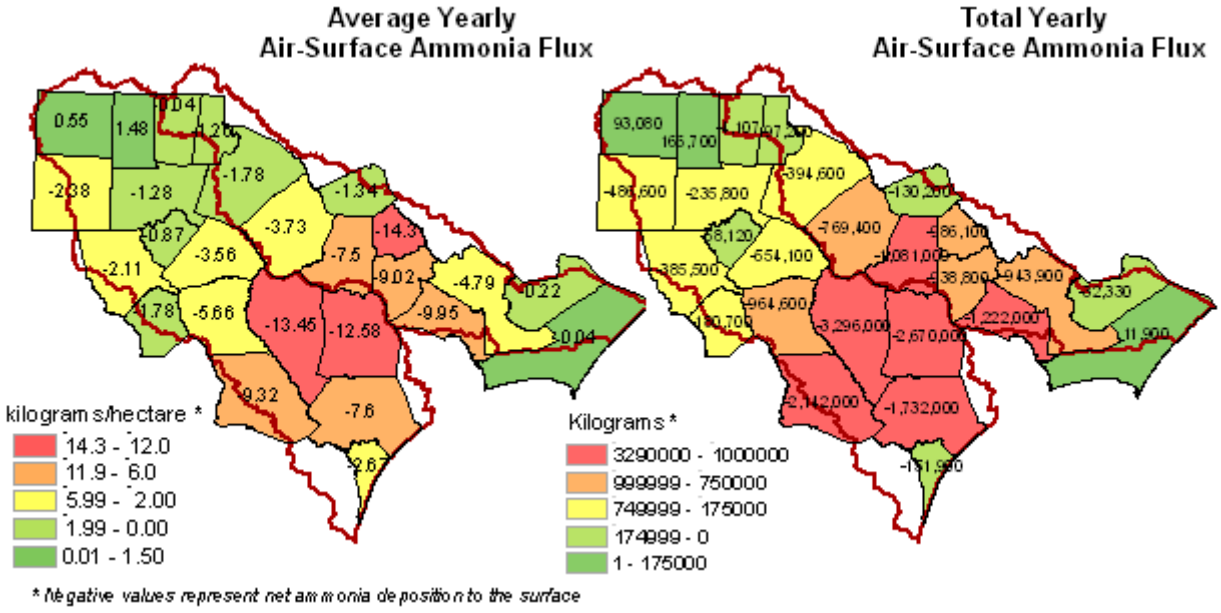

Within the Neuse and Cape Fear basins, forest and cultivated crops cover half the watershed area, accounting for 34.4% and 15.5% of total land area, respectively. These areas generally run parallel to the coast with forest dominating the upper part of both basins and cultivated crops dominating the lower-to-middle section of the watersheds (Figure 19). Though largely cultivated, the lower-to-mid region of the basins also coincides with the highest density of animal facilities. Mixed in with the forested region are grasslands and pasture, totaling ≈ 16 % of the basin area. Woody wetlands, which are generally located along the coast and river banks, also cover a significant portion of the river basins (14%). Developed areas cover ≈ 10% of the study area and are located primarily in the northwestern portion of the basins. However, somewhat smaller developed areas dot the middle and lower coastal region of the study area mainly along the major interstates.

Figure 19: Land use classifications used in the air-surface exchange model for the Neuse and Cape Fear river basins.

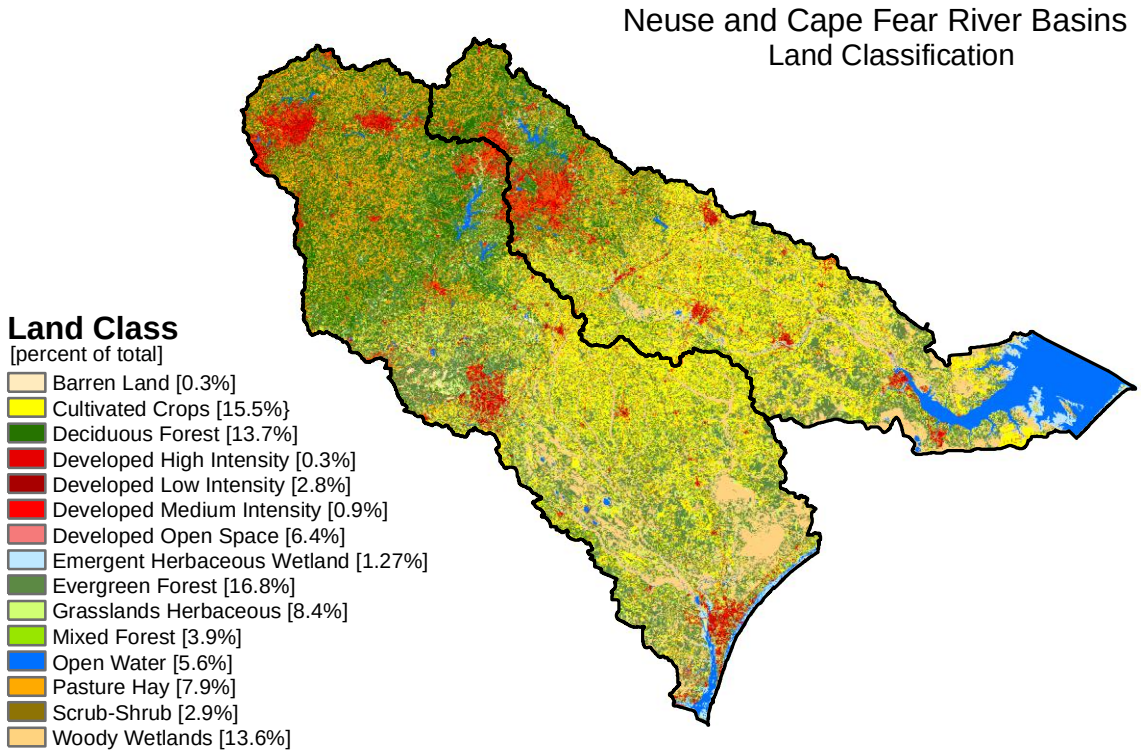

Fluxes are summarized by land use category in Table 7. On a total mass basis, total flux is driven by total area of individual land use categories. On an annual scale, NH_3 is deposited to low nitrogen systems (forests, wetlands) and emitted from high nitrogen (fertilized) systems (cultivated crops, pasture).

Table 7: Summary of seasonal dry NH_3 flux predicted by the air-surface exchange model by land cover classification. Negative values represent deposition to the surface, positive values represent emission from the canopy to the atmosphere.

	Percent of Study Area	Spring *[kg]* *[kg ha^{-1}]*	Summer *[kg]* *[kg ha^{-1}]*	Fall *[kg]* *[kg ha^{-1}]*	Winter *[kg]* *[kg ha^{-1}]*	Total *[kg]* *[kg ha^{-1}]*
Open Water	5.2	-8,038 -0.04	-10,544 -0.05	-8,321 -0.04	-3,582 -0.20	-30,485 -0.15
Developed	10.5	-551,939 -1.31	-756,971 -1.80	-575,709 -1.37	-243,725 -0.58	-2,128,344 -5.05
Barren Land	0.3	-13,361 -1.11	-19,459 -1.62	-13,754 -1.15	-5,719 -0.48	-52,293 -4.36
Forest	34.4	-2,637,203 -1.90	-3,948,776 -2.85	-2,738,331 -1.98	-1,158,465 -0.84	-10,482,774 -7.56
Scrub-Shrub	2.9	-316,324 -2.70	-459,752 -3.92	-327,042 -2.79	-141,136 -1.20	-1,244,255 -10.6
Grasslands	8.4	-786,887 -2.33	-1,091,088 -3.23	-808,258 -2.39	-347,875 -1.03	-3,034,108 -8.97
Pasture Hay	8.0	310,221 0.97	1,407,668 4.39	287,272 0.90	86,026 0.27	2,091,188 6.53
Cultivated Crops	15.5	-488,701 -0.78	1,459,696 2.33	-543,404 -0.87	-351,006 -0.56	76,585 0.12
Wetlands	14.9	-1,455,131 -2.42	-2,198,099 -3.66	-1,508,148 -2.51	-640,840 -1.07	-5,802,218 -9.66
TOTALS	100.0	-5,947,362	-5,617,324	-6,235,695	-2,806,322	-20,606,704

Comparing across seasons and land use categories, fluxes per unit area illustrate the interactions between emissions from animal facilities, air concentrations, and surface compensation points. An example is shown in Figure 20. Near animal production facilities, atmospheric NH_3 concentrations are relatively high and follow the temporal pattern of higher emissions during the summer and lower emissions during the winter, reflecting the positive exponential relationship between emissions from animal manure and temperature.

Figure 20: Seasonal fluxes by land use category at high and low atmospheric NH_3 concentrations. Negative values represent deposition.

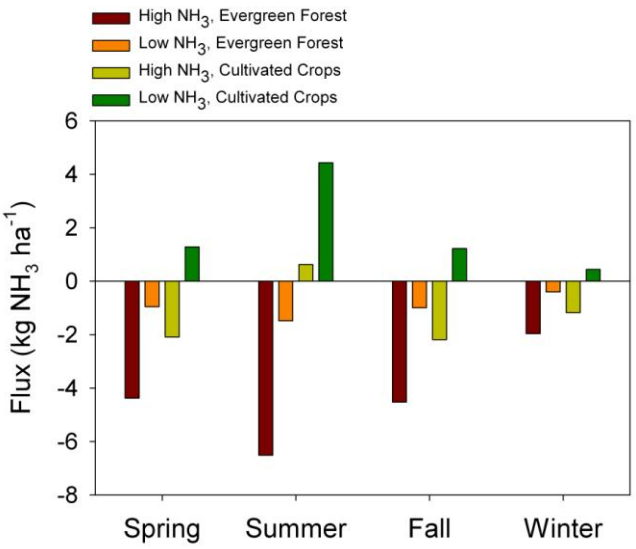

Under this scenario, the atmospheric concentration exceeds the surface compensation point of low nitrogen systems (Figure 20, high NH_3, evergreen forest) and deposition rates subsequently follow the temporal pattern of air concentrations. Conversely, high nitrogen systems experience much higher compensation points, which also follow an exponential dependence on temperature (highest in the summer). Thus the temporal pattern of fluxes (Figure 20, high NH_3, cultivated crops) in high nitrogen systems near animal production facilities reflects the influence of higher compensation points, yielding reduced deposition rates in the fall, winter, and spring, and net emissions in the summer. Further away from animal production facilities, much lower NH_3 air concentrations only slightly exceed the canopy compensation point in low nitrogen systems (Figure 20, low NH_3, evergreen forest), resulting in much lower fluxes during all seasons. In high nitrogen systems in these more distant areas, the canopy compensation point exceeds the air concentration during all seasons (Figure 20, low NH_3, cultivated crops), yielding a seasonal pattern of net emissions dependent on the temperature dependence of the canopy compensation point.

Total deposition to both river basins was 20.6 million kg NH_3 on an annual scale, which represents 36% of total emissions calculated from the SEADE emissions inventory and 27% of total emissions calculated from the NCDAS database. Thus, the majority of NH_3 emitted within the two river basins is either wet deposited or transported out of the river basins.

3.5 NITROGEN DEPOSITION BUDGET FOR THE NEUSE AND CAPE FEAR RIVER BASINS

To put our modeled deposition estimates into context, we present a nitrogen deposition budget for the Neuse/Cape Fear River basins (Table 8). The annual total N deposition budget (Spring, 2007 – Spring, 2008) comprises dry deposition of nitric acid (HNO_3) and other oxidized nitrogen, NH_3, inorganic N in particulate matter (PM) [ammonium (NH_4^+) and nitrate (NO_3^-)], and organic nitrogen in particulate matter; wet deposition includes NH_4^+, NO_3^-, and organic N. HNO_3, dry NH_4^+, and dry NO_3^- deposition estimates are averages from Clean Air Status and Trends Network sites located at Beaufort, NC (BFT142) and Candor, NC (CND125) (CASTNet, 2010), taken over the same period as the measurements used to develop and evaluate the NH_3 dry deposition model presented here. Dry deposition of other oxidized N is estimated assuming HNO_3 represents 57% of the total oxidized nitrogen flux (Sparks et al., 2008). Organic N in PM was estimated by assuming organics represent 33% of total PM nitrogen (Lin et al., 2010). Dry deposition of NH_3 was taken as the average modeled flux for both watersheds. Wet deposition of NH_4^+ and NO_3^- represents averages from NADP sites located at Raleigh, NC (NC41), Clinton, NC (NC35), Hoffman Forest, NC (NC29), and Beaufort, NC (NC06) (NADP, 2010). Wet deposition of organic nitrogen was estimated by assuming organics represent 32% of total N in precipitation (Whitall and Paerl, 2001).

Dry deposition of NH_3 dominates the average watershed-scale deposition budget, exceeding dry deposition of NH_4^+, its aerosol reaction product, and wet deposition of NH_4^+ by factors of 17 and 2, respectively. However, the ratio of dry NH_3 to dry NH_4^+ may be overestimated because there are no CASTNet sites within the highest NH_3 emission region, where NH_4^+ concentrations, and therefore deposition fluxes, are expected to be higher (Walker et al., 2004). On average, dry deposition dominates over wet deposition, contributing 56% of 13.65 kg N ha^{-1} y^{-1} total N deposition. However, because the majority of compounds contributing to total N deposition are secondary reaction products and therefore spatially more uniform at the watershed scale than NH_3, the relative contribution of NH_3 to the total deposition budget will exhibit the same degree of spatial variability as the NH_3 flux. Thus, over areas within the watersheds where NH_3 concentrations and deposition fluxes are low, wet NH_4^+ deposition and dry deposition of oxidized nitrogen will exceed NH_3 dry deposition.

Table 8: Atmospheric nitrogen deposition budget for the Cape Fear and Neuse River Basins.

		Deposition kg N ha^{-1} y^{-1}	% total
Dry	HNO_3[a]	1.1	8.1
	Other Oxidized gas phase$N$[b]	0.83	6.1
	NH_4^{+a}	0.3	2.2
	NO_3^{-a}	0.11	0.8
	PM organic N[c]	0.21	1.5
	NH_3	5.11	37.4
Wet	NH_4^{+d}	2.47	18.1
	NO_3^{-d}	1.54	11.3
	Organic N[e]	1.98	14.5
Total Dry		7.66	56.1
Total Wet		5.99	43.9
Total		**13.65**	

a Averages from Candor, NC and Beaufort, NC CASTNet sites.
b Assumes HNO_3 contributes 57% of total oxidized N dry deposition (Sparks et al., 2008).
c Assumes aerosol organic N contributes 33% of total aerosol N (Lin et al., 2010).
d Averages from Beaufort, NC, Clinton, NC, Raleigh, NC and Hoffman Forest, NC NADP sites.
e Assumes organics contribute 32% of total N in precipitation (Whitall and Paerl, 2001).

3.6 MODEL UNCERTAINTY AND SENSITIVITY

Uncertainty in the predicted air-surface exchange of ammonia were assessed using a sensitivity analysis that varied model parameters based on known variability and sensitivity to model output. In particular, the land use parameters controlling the stomatal compensation (χ_s) and soil/water compensation (χ_g) points (Section 2.1.3) were varied by 1/2x and 2x the expected values. The parameters RIC_{min} and R_{smin} were modified independent of the emission potential (Γ) and all results evaluated against Model I predictions.

Results indicate that on average and between seasons, that reducing RIC_{min} and R_{smin} by 1/2 results in a corresponding average reduction in deposition around 11%. Between seasons, the amount of deposition reduced varied from 19% in the summer to 7% in the winter. In contrast, doubling RIC_{min} and R_{smin} results in an seasonal average increase in deposition of approximately 20%. The between season averages ranged from 36% increase in deposition during the summer to 13% in the winter. Results from decreasing the emission potential (Γ) by 2x reveal a

corresponding average seasonal decrease in deposition of around 92%. Between seasons, the range of modeled predictions remained constant ranging from a 94% reduction in the summer to 90% reduction in the fall (Table 9).

As evident from these results, the air-surface exchange of NH_3 is very sensitive to the emission potential (Γ), which drives the soil/foliage compensation points. On a seasonal basis, this model attempts to represent the compensation points using a single, averaged value and thus ignoring seasonal variability in soil/vegetation nitrogen status.

Table 9: Uncertainty in the predicted air-surface exchange of ammonia.

	Parameter varied by 1/2x		Parameter varied by 2x	
	RIC_{min} and R_{smin}	Γ	RIC_{min} and R_{smin}	Γ
Duplin	-8.2%	-92.4	13.8%	73.2%
Sampson	-19.0%	-94.1%	36.2%	74.1%
Bladen	-9.6%	-90.8%	16.3%	69.1%
Wayne	-7.8%	-92.4%	13.1%	80.2%

4. FUTURE WORK

In this analysis we have identified three priorities areas for improving air concentration and flux estimates which will be the focus of Phase II of the development of the SEADE model, which are described below.

1. Further refinement of the emissions inventory would enable more accurate prediction of NH_3 air concentrations. Specifically, we will attempt to add poultry facilities to the emissions inventory by working with county extension offices to identify the location, types, and sizes of poultry facilities. A secondary objective is to develop a more refined protocol for splitting large swine facilities into multiple emission complexes, which will reduce the influence of a small number of very large facilities.

2. The model presented here is limited in its ability to predict ground level air concentrations due to a relatively small number of measurement sites available for development and evaluation. Additional concentration measurements were taken at 25 different sites in 2008 – 2009. The next version of the model will employ these additional data for development and testing of the air concentration model. We will also examine the usefulness of including the Lizzie dataset, from which Model I was developed, in the construction and validation of Models II and III.

3. Additional testing will be performed to optimize the implementation of the air concentration model. As described above the model produces a distribution of air concentrations at each model grid point consisting of N observations equal to the number of animal facilities within the model domain. Currently only the maximum concentration is retained, assuming that the nearest animal facility dominates the seasonal average concentration. Forthcoming analyses will examine other approaches, such as a summed concentration weighted by distance to the corresponding facility.

4. In addition to the semi-empirical models presented here, future analyses will compare concentration predictions from traditional Gaussian and Lagrangian dispersion models.

5. REFERENCES

Asman, W. A. H., 1992. National Institute of Public Health and Environmental Protection.
Ayers, G. P., 2002. *Atmos. Eviron.*, 35, 2432-2425.
Bilthoven, the Netherlands 1992.
Bouwman, A.F., *et. al.*, 1997. *Global Biogeochemical Cycles*, 11, 561-587.
Burkholder, J.M., *et al.*, 2005. *Water Resources Research Institute*.
Burkholder *et al*., 2005. *Limnol. Oceanogr*. 51, 463 - 487.
CASTNet, 2010. Clean Air Status and Trends Network. http://www.epa.gov/castnet/
Cooter, E.J., and Schwede, D.B., 2000. *J. Geophys. Res.* 105, 6695 – 6707.
Cooter, E.J., *et al.*, 2010. *Atmos. Environ.*, in press.
Currie, L., 1999. *Analytica Chimica Acta*, 391, 105 – 126.
Dawson, G.A., 1977. *J. Geophys. Res.* 82, 3125 – 3133.
Deerhake *et al.*, 2006. Proceedings of the Workshop on Agricultural Air Quality: State of the Science. 250 – 258.
Duyzer, J. H., *et al.*, 1992. *Environ. Poll*. 75, 3 – 13.
Farquhar, G.D., *et al.*, 1980. *Plant Physiol*. 66, 710 – 714.
Flechard, C.R., Fowler, D., 1998. *Quart. J. Roy. Met. Soc.* 124, 759 – 791.
Flechard, C.R., *et al.*, 1999. *Quart. J. R. Meteorol. Soc.* 125, 2611 – 2641.
Fowler, D., Unsworth, M. H., 1979. *Q. J. R. Meteorol. Soc.* 105, 767 – 783.
Hastie T., R. Tibshirani and J. Friedman, The elements of statistical learning: data mining, inference and prediction. , Springer-Verlag, New York (2001) 14 .
Hicks, B. B., *et al.*, 1987. *Water Air Soil Pollut.* 36, 311 – 330.
Husted, S., Schjoerring, J. K., 1995. Plant *Physiol.* 109, 1453 – 1460.
Jones, M.R., *et al.*, 2007. *Atmos. Environ.*, 41, 2049 – 2060.
Lin, M., *et al.*, 2009. *Atmos. Chem. Phys. Discuss.*, 9, 17157-17181.
Massman, W. J., 1998. *Atmos. Environ.*, 32, 1111 – 1127.
Meyers, T.P., *et al.*, 1998. *J. Geophys. Res*. 103, 22645 - 22661.
Nemitz, E., et al, 2000. *Agric. For. Meteorol*. 105, 405 – 425.
Nemitz, E., *et al.*, 2001. *Quart. J. Roy. Met. Soc*. 127, 815 – 833.
NADP, 2010. National Atmospheric Deposition Program. http://nadp.sws.uiuc.edu/
NCDWQ, 2007. North Carolina Division of Water Quality
NCDACS, 2007. North Carolina Department of Agriculture and Consumer Services
NCSCO, 2007. North Carolina State Climate Office. http://www.nc-climate.ncsu.edu/
NLCD, 2001. National Land Cover Data. http://www.mrlc.gov/
Nihlgard, B., 1985. *Ambio*, 14, 2-8.
Padgett, P., *et al.*, 1999. *Atmos. Environ*., 33, 769-781.
Paerl, H.W., 1995. *Ophelia*, 41, 237-259.
Paerl, H.W., 1997. *Limnol. Oceanogr*. 42, 1154 – 1165.
Paerl, H.W., Whitall, D.R., 1999. *Ambio*, 28, 307-311.
Perrino, C., *et al.*, 2001. *Atmos. Environ.*, 35, 331-341.
Qian et al., 2000. *Environ. Sci. Technol*. 34, 4474 – 4482.
Robarge, W.P., *et al.*, 2002. *Atmos. Environ*., 36, 1661-1674.
Roelofs, J.G.M., *et al.*., 1985. *Plant and Soil*, 84, 45-56.
Schjoerring, J. K., *et al.*, 1998. *Atmos. Environ*. 32, 491 – 498.
Schuepp, P.H., 1977. *Bound.-Lay. Meteorol*. 12, 171 – 186.

Sievering, H., 1999. *Nature*, 400, 629-630.
Sievering, H., *et al.*, 2000. *Glob. Biogeochem. Cyc*, 14, 1153-1160.
Sparks *et al.*, 2008. *Glob. Ch. Biol.*, doi: 10.1111/j.1365-2486.2007.01526.x.
Sutton, M.A., *et al.*, 1997. Gaseous Exchange with Grassland Systems. Wallingford, Oxon, UK, 131 – 139.
Sutton, M.A., *et al.*, 2001 *Water, Air, and Soil Pollution: Focus 1*, 145–156.
Tang, Y.S., *et al.*, 2001. *Sci. World* 1, 513 – 529.
Tang, Y.S., *et al.*, 2009. Center for Ecology and Hydrology, Edinburgh.
U. S. Environmental Protection Agency. Compendium Method IO-42: Determination of Reactive Acidic and Basic Gases and Strong Acidity of Fine-Particles (<2.5 μm). EPA/625/R-96010a; U.S. EPA: Cincinnati, OH, 1997.
van der Hoek, K. W., 1998. *Atmos. Environ*., 32, 315-316.
Walker, J.T., *et al.*, 2008. *Atmos. Environ*., 42, 3407 – 3418.
Walker, J.T., *et al.*, 2006. *Agric. For. Meteorol*. 138, 54 - 68.
Walker, J.T., *et al.*, 2000a. *Environ. Sci. Technol*., 34, 3527-3534.
Walker, J.T., *et al.*, 2000b. *Atmos. Environ*., 34, 3407-3418.
Weseley, M. L., 1989. *Atmos. Environ*. 23, 1293 – 1304.
Whitall, D.R., Paerl, H.W., 2001. *J. Env. Qual*., 30, 1508-1515.
Yamartino, R.J. 1984. Journal of Climate and Applied Meteorology 23: 1362–1366.
Zhang, L., *et al.*, 2003. *Atmos. Chem. Phys*. 3, 2067 – 2082.
Zou et al., 2006 X. Zou, Z. Shen, T. Yuan, S. Yin, J. Cai, L. Chen and W. Wang, *Atmospheric Environment* **40** (2006), pp. 8068–8073.

APPENDIX

Table 10: CAMNet stations used to calibrate and validate the concentration component of the SEASE Model.

Set	Site	Closest Facility	Animals	Distance (m)	Model Use
1	P15	Poultry	120000	4404	Calibration
1	P12	Poultry	90000	3731	Calibration
1	P1	Poultry	120000	2365	Validation
2	S14	Swine	2480	1956	Calibration
2	S7	Swine	2844	1567	Validation
2	S19	Swine	3552	1498	Calibration
3	S3	Swine	3720	1365	Calibration
3	S13	Swine	5880	1187	Validation
3	S24	Swine	5200	1130	Calibration
4	S10	Swine	2068	1057	Calibration
4	S22	Swine	800	878	Validation
4	S9	Swine	3500	781	Calibration
5	S5	Swine	27280	650	Validation
5	P20	Poultry	120000	617	Calibration
5	P8	Poultry	360000	598	Calibration
6	S4	Swine	27280	489	Validation
6	P23	Poultry	180000	479	Calibration
6	P11	Poultry	240000	432	Calibration
7	S21	Swine	2448	423	Validation
7	P16	Poultry	180000	404	Calibration
7	S18	Swine	1240	388	Calibration
8	P17	Poultry	120000	382	Validation
8	S2	Swine	3124	379	Calibration
8	P6	Poultry	240000	64	Calibration

Table 11: Emission factors used to develop inventory for eastern North Carolina (Asman, 1992)

Source	Amount	
humans	0.44	kg NH_3 $person^{-1}$ yr^{-1}
cars	0.000013455	kg NH_3 car^{-1} yr^{-1}
trucks	0.000068262	kg NH_3 $truck^{-1}$ yr^{-1}
milk cows	39.72	kg NH_3 cow^{-1} yr^{-1}
beef cows	39.72	kg NH_3 cow^{-1} yr^{-1}
heifers	13.04	kg NH_3 $heifer^{-1}$ yr^{-1}
steers	8.22	kg NH_3 $steers^{-1}$ yr^{-1}
hogs	*see page 3*	kg NH_3 hog^{-1} yr^{-1}
horses	12.2	kg NH_3 $horse^{-1}$ yr^{-1}
pullets	0.17	kg NH_3 $pullets^{-1}$ yr^{-1}
layers	0.305	kg NH_3 $layer^{-1}$ yr^{-1}
broilers	0.167	kg NH_3 $broiler^{-1}$ yr^{-1}
turkeys	0.858	kg NH_3 $turkey^{-1}$ yr^{-1}

Table 12: Land use specific inputs by season used in the air-surface exchange.

Land Use	GL				GS				LAI				RICmin				Rsmin			
	Spr	Sum	Fall	Win	Spr	Sum	Fall	Win	Spr	Sum	Fall	Win	Spr	Sum	Fall	Win	Spr	Sum	Fall	Win
Open Water	200	200	200	200	200	200	200	200	0	0	0	0	10	10	10	10	9999	9999	9999	9999
Developed Open Space	100	100	100	100	250	250	250	250	0.1	0.1	0.1	0.1	200	200	200	200	100	100	100	100
Developed Low Intensity	250	250	250	250	2500	2500	2500	2500	1	2	1	0.5	200	200	200	200	150	150	150	150
Developed Medium Intensity	250	250	250	250	1000	1000	1000	1000	0.6	1.5	0.6	0.3	200	200	200	200	150	150	150	150
Developed High Intensity	250	250	250	250	250	250	250	250	0.4	1	0.4	0.2	200	200	200	200	150	150	150	150
Barren Land	100	100	100	100	200	200	200	200	0.5	0.5	0.5	0.2	30	30	30	30	100	100	100	100
Unconsolidated Shore	100	100	100	100	200	200	200	200	0.1	0.1	0.1	0.1	30	30	30	30	100	100	100	100
Deciduous Forest	100	100	100	100	200	200	200	200	3	5	3	1	200	200	200	200	200	200	200	200
Evergreen Forest	100	100	100	100	200	200	200	200	3.5	4	3.5	3	200	200	200	200	175	175	175	175
Mixed Forest	100	100	100	100	200	200	200	200	3.5	5	3.5	2	200	200	200	200	200	200	200	200
Scrub-Shrub	100	100	100	100	200	200	200	200	2	3	2	1	100	100	100	100	200	200	200	200
Grasslands Herbaceous	100	100	100	100	200	200	200	200	1.75	2.5	1.75	1	30	30	30	30	100	100	100	100
Pasture Hay	1000	1000	1000	1000	10000	10000	10000	10000	1.75	3	1.75	0.5	30	30	30	30	70	70	70	70
Cultivated Crops	1000	1000	1000	1000	10000	10000	10000	10000	1.75	3	1.75	0.5	30	30	30	30	70	70	70	70
Small Grains	1000	1000	1000	1000	10000	10000	10000	10000	1.75	3	1.75	0.5	30	30	30	30	70	70	70	70
Fallow	250	250	250	250	1500	1500	1500	1500	0.1	0.1	0.1	0.1	30	30	30	30	100	100	100	100
Urban Recreational Grasses	500	500	500	500	2500	2500	2500	2500	1.75	2.5	1.75	1	30	30	30	30	100	100	100	100
Woody Wetlands	100	100	100	100	200	200	200	200	4	5	4	3	200	200	200	200	200	200	200	200
Emergent Herbaceous Wetland	100	100	100	100	200	200	200	200	1.5	2	1.5	1	30	30	30	30	164	164	164	164

Figure 21: Concentration versus distance to the nearest animal facility for the 24 CAMNet stations used to calibrate and validate the SEADE model. Figures are provided for each of the four seasons.

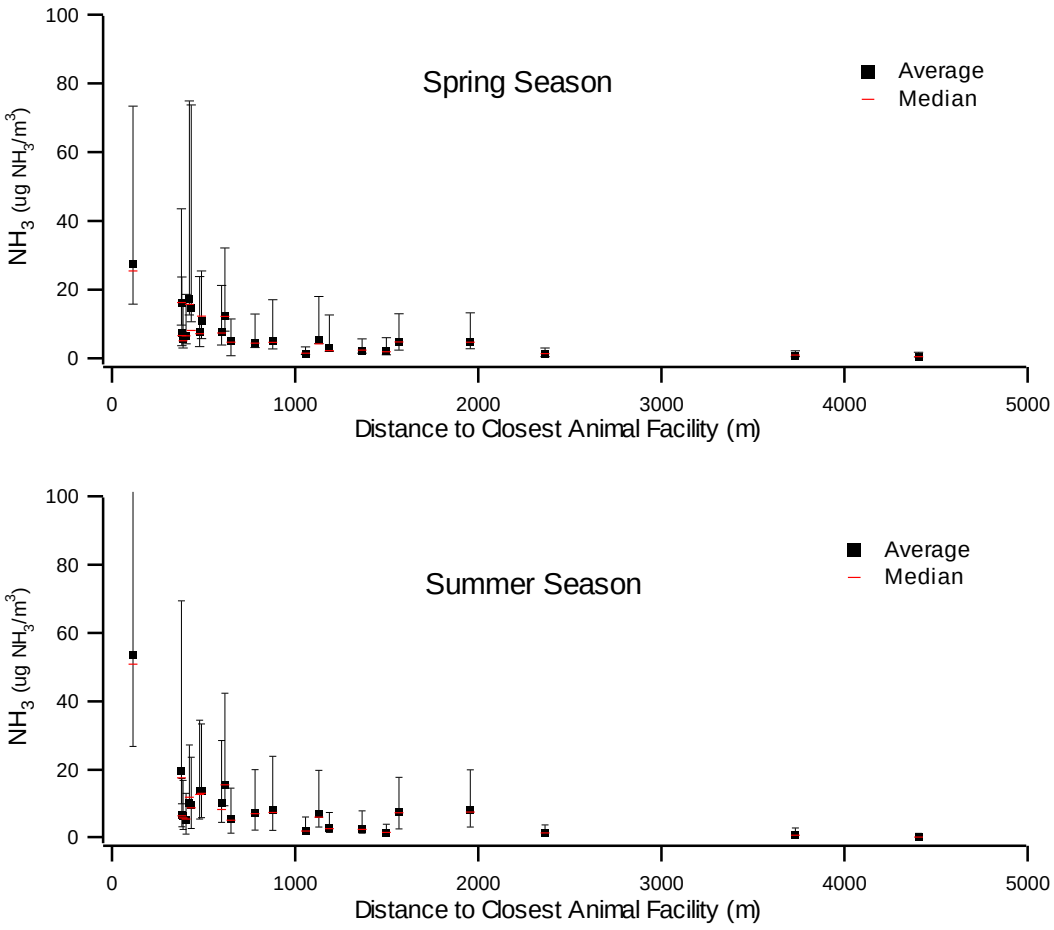

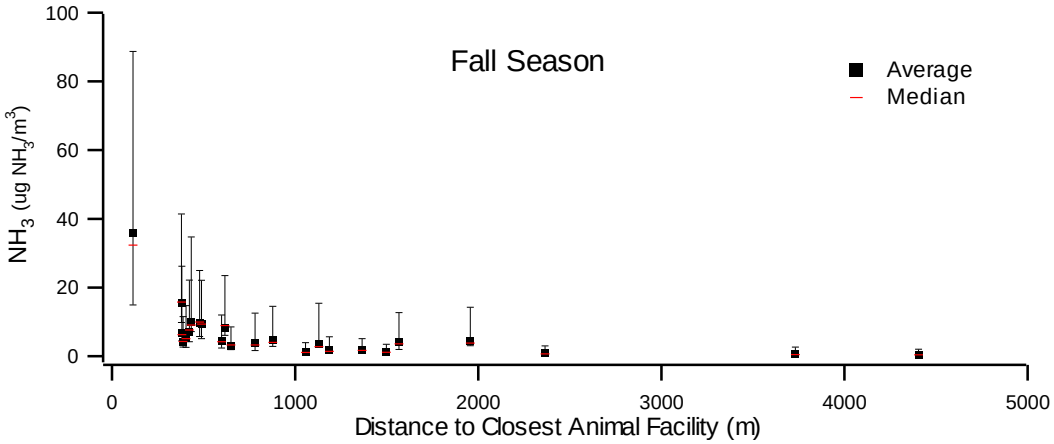
Fall Season
Average
Median
NH_3 (ug NH_3/m^3)
0
20
40
60
80
100
0
1000
2000
3000
4000
5000
Distance to Closest Animal Facility (m)

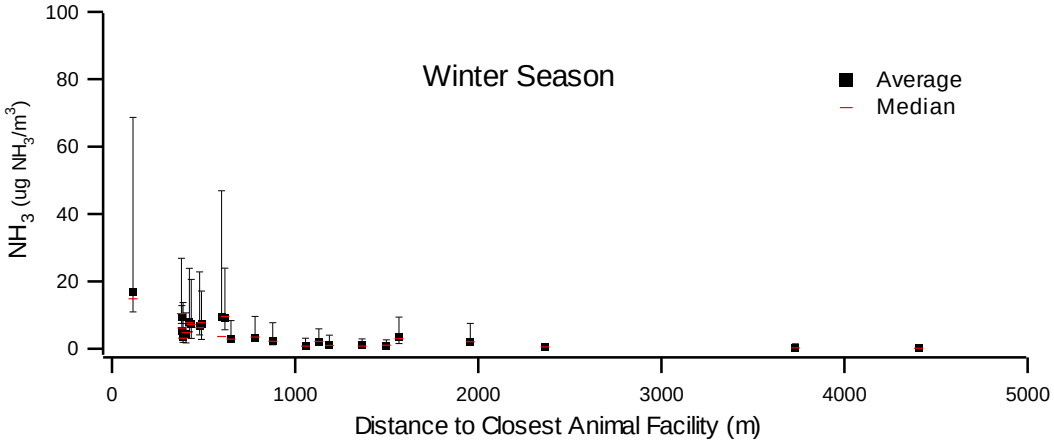
Winter Season
Average
Median
NH_3 (ug NH_3/m^3)
0
20
40
60
80
100
0
1000
2000
3000
4000
5000
Distance to Closest Animal Facility (m)